OPEN ACCESS Freely available online

PLoS one

Mitochondrial Ca^{2+} Overload Underlies Aβ Oligomers Neurotoxicity Providing an Unexpected Mechanism of Neuroprotection by NSAIDs

Sara Sanz-Blasco[1], Ruth A. Valero[1], Ignacio Rodríguez-Crespo[2], Carlos Villalobos[1]*, Lucía Núñez[1]

1 Instituto de Biología y Genética Molecular (IBGM), Universidad de Valladolid and Consejo Superior de Investigaciones Científicas (CSIC), Valladolid, Spain, **2** Departamento de Bioquímica y Biología Molecular, Facultad de Ciencias Químicas, Universidad Complutense de Madrid, Madrid, Spain

Abstract

Dysregulation of intracellular Ca^{2+} homeostasis may underlie amyloid β peptide (Aβ) toxicity in Alzheimer's Disease (AD) but the mechanism is unknown. In search for this mechanism we found that $A\beta_{1-42}$ oligomers, the assembly state correlating best with cognitive decline in AD, but not Aβ fibrils, induce a massive entry of Ca^{2+} in neurons and promote mitochondrial Ca^{2+} overload as shown by bioluminescence imaging of targeted aequorin in individual neurons. Aβ oligomers induce also mitochondrial permeability transition, cytochrome c release, apoptosis and cell death. Mitochondrial depolarization prevents mitochondrial Ca^{2+} overload, cytochrome c release and cell death. In addition, we found that a series of non-steroidal anti-inflammatory drugs (NSAIDs) including salicylate, sulindac sulfide, indomethacin, ibuprofen and R-flurbiprofen depolarize mitochondria and inhibit mitochondrial Ca^{2+} overload, cytochrome c release and cell death induced by Aβ oligomers. Our results indicate that i) mitochondrial Ca^{2+} overload underlies the neurotoxicity induced by Aβ oligomers and ii) inhibition of mitochondrial Ca^{2+} overload provides a novel mechanism of neuroprotection by NSAIDs against Aβ oligomers and AD.

Citation: Sanz-Blasco S, Valero RA, Rodríguez-Crespo I, Villalobos C, Núñez L (2008) Mitochondrial Ca^{2+} Overload Underlies Aβ Oligomers Neurotoxicity Providing an Unexpected Mechanism of Neuroprotection by NSAIDs. PLoS ONE 3(7): e2718. doi:10.1371/journal.pone.0002718

Editor: Ernest Greene, University of Southern California, United States of America

Received April 1, 2008; **Accepted** June 20, 2008; **Published** July 23, 2008

Funding: This work was supported by public, competitive grants from the spanish Instituto de Salud Carlos III (PI04/1510 and PI07/0766), Junta de Castilla y León (VA022A05), Ministerio de Educación y Ciencia (MEC, BFU2006-05202) and Consejo Superior de Investigaciones Científicas (CSIC). None of the funding agencies have any role in the design and conduct of the study, collection, analysis or interpretation of the data nor the preparation review or approval of the manuscript.

Competing Interests: The authors have declared that no competing interests exist.

* E-mail: carlosv@ibgm.uva.es

Introduction

Alzheimer's Disease (AD) is a devastating neurodegenerative disorder due to a massive neuron dysfunction and loss related to development of senile plaques that are made of amyloid β peptide (Aβ), a cleavage product of the amyloid precursor protein. Early affected areas in the brain are the cortex and hippocampus. However, neuropathological studies show frequent and varied cerebellar changes in the late stages of the disease [1]. In fact, the cerebellum has been shown to be a unique organ in terms of AD manifestations because it is virtually free of neurofibrillary pathology but there is an strong correlation between cerebellar atrophy -with large cell death in the granular layer- and duration and stage of AD [1]. Although many *in vitro* studies have been carried out using cortical and hippocampal neurons, cerebellar granule cells have been also used for studies of Aβ neurotoxicity [2–4]. Several mechanisms have been envisioned. First, the "inflammatory hypothesis" proposes that Aβ may promote a damaging inflammation reaction. This view is supported among other evidence by the neuroprotection afforded by NSAIDs [5]. Second, Aβ promotes mitochondrial dysfunction and apoptosis and this toxicity contributes to AD [6] but the mechanism is unclear. Aβ may associate with mitochondrial membranes in mutant mice and patients with AD and mitochondria from mutant mice show lower levels of oxygen consumption and reduced respiratory complex-associated enzymatic activity suggesting that mitochondria-bound Aβ may impact on mitochondrial activity [7–9]. Finally, AD has been also related to a general dyshomeostasis of intracellular Ca^{2+}, a key second messenger involved in multiple neuronal functions. This view is supported by reports on dysregulation of intracellular Ca^{2+} promoted by Aβ and mutant presenilins [10]. Aβ may promote Ca^{2+} entry into neurons but results are controversial [11,12]. Part of the controversy may relate to the fact that Aβ toxicity depends on its assembly state that varies from monomers to small, soluble oligomers and fibrils [13]. Small assemblies (oligomers) of unmodified Aβ are becoming the proximate neurotoxin in AD [13,14], but most studies used fibrils. Intracellular Ca^{2+} levels are important for AD since overexpression of calbindin28k, an endogenous Ca^{2+} buffer, prevents neuron death in AD models [15]. However the link between putative changes in intracellular Ca^{2+} and cell damage is unknown. A rise in mitochondrial Ca^{2+} concentration ($[Ca^{2+}]_{mit}$) might contribute to neurotoxicity but monitoring $[Ca^{2+}]_{mit}$ in individual neurons has been challenging. We have addressed the effects of Aβ assembly state on Ca^{2+} influx and mitochondrial Ca^{2+} uptake using photon counting imaging of neurons expressing targeted aequorin [16]. We found that only oligomers, but not fibrils, increased cytosolic and mitochondrial Ca^{2+} concentrations. Accordingly we asked for the role of mitochondrial Ca^{2+} uptake on neurotoxicity induced by Aβ oligomers. Finally, we tested

whether NSAIDs may protect against Aβ toxicity acting on subcellular Ca^{2+} fluxes. For these studies we have used mainly cerebellar granule cells although some experiments have been also carried out in cortical and hippocampal neurons.

Results

Aβ oligomers but not fibrils induce entry of Ca^{2+} into neurons

We have used the protocol reported by Klein [17] to prepare oligomers and fibrils from $A\beta_{1-42}$ obtained from a commercial source (Bachem). Since the standard protocol of preparation includes a precipitation step in which some protein sample is lost, we hydrolyzed an aliquot of the final solution of both oligomers and fibrils in order to carry out an amino acid analysis. This procedure allowed us to obtain the real concentration of these compounds in solution. In the second place we characterized the quaternary structure (dimers, trimers, tetramers, etc.) of both the oligomers and fibrils using non-denaturing SDS-PAGE (pseudo-native gels). We were unable to stain the $A\beta_{1-42}$ peptides using Coomassie blue even when 2 μg of peptide were loaded per lane (data not shown). However, using silver staining we were able to determine the presence of high-molecular mass species in the SDS-PAGE. We rationalized that despite the fact that the samples were not boiled, a significant population of protein-protein interactions might be lost in the presence of SDS. However, were able to clearly identify monomers, dimers and tetramers in our preparation of oligomers (Figure S1A). This migration pattern of $A\beta_{1-42}$ oligomers in SDS-PAGE gels is well characterized [18]. When the preparation of fibrils was analyzed by SDS-GEL and silver staining, we could unambiguously identify the presence of monomers, dimers, trimers, tetramers and some larger oligomerization species in the gel. In addition, a certain amount of large molecular weight fibrils appeared at the top, incapable of entering the separating gel (Figure S1B). Similar results were obtained when the gel was transferred to a nitrocellulose membrane and the distribution of high-molecular mass species was determined by Western-blot using a monoclonal antibody raised against $A\beta_{1-42}$ (data not shown). In the third place, electron microscopy was used in order to characterize our $A\beta_{1-42}$ fibrils. Negative staining using uranyl acetate undoubtedly showed the presence of large fibrils in solution (Figure S1C). Most of these fibrils were similar in width and with a length that usually varied between 200 and 800 nm.

Once Aβ preparations were characterized, we studied the effects of oligomer and fibril preparations on $[Ca^{2+}]_{cyt}$. As a positive control, we used also the toxic fragment $A\beta_{25-35}$ at large concentrations (20 μM) that have been shown previously to be neurotoxic and produce large increases in $[Ca^{2+}]_{cyt}$ in several neuron models including GT1 neural cells [19]. The effects of $A\beta_{1-42}$ oligomers, $A\beta_{1-42}$ fibrils and the toxic fragment $A\beta_{25-35}$ (a surrogate of Aβ) on cytosolic Ca^{2+} concentration ($[Ca^{2+}]_{cyt}$) were tested by fluorescence microscopy (Fig. 1). We find that $A\beta_{25-35}$ increases $[Ca^{2+}]_{cyt}$ in both GT1 neural cells (Fig. 1A) and cerebellar granule cells (Fig. 1B). In both cell types, increases in $[Ca^{2+}]_{cyt}$ are heterogeneous and show different lags and kinetics. In about two thirds of the cells, $[Ca^{2+}]_{cyt}$ remain increased even after washout of the peptide. The increase in $[Ca^{2+}]_{cyt}$ induced by $A\beta_{25-35}$ is abolished in medium lacking extracellular Ca^{2+} and the responses resume after restoring extracellular Ca^{2+} (Fig. 1C) suggesting that $A\beta_{25-35}$ promotes entry of Ca^{2+} rather than release from intracellular Ca^{2+} stores. Cerebellar granule cells responded also to high K^+ medium (K) after $A\beta_{25-35}$ (Fig. 1C). Next we tested the effects of $A\beta_{1-42}$ in its different assembly states (fibrils and oligomers) prepared from synthetic $A\beta_{1-42}$ [17,20] in cerebellar granule cells. It has been reported that $A\beta_{1-42}$ fibrils are less toxic than $A\beta_{1-42}$ oligomers but produce the same toxicity when used at larger concentrations [13]. For example, at concentrations of about 5 μM, $A\beta_{1-42}$ fibrils are equally toxic than $A\beta_{1-42}$ oligomers at concentrations ranking 100 nM–1 μM. We found that, at 500 nM, $A\beta_{1-42}$ fibrils induce no $[Ca^{2+}]_{cyt}$ increase (data not shown). At 2 μM, $A\beta_{1-42}$ fibrils induce little or no $[Ca^{2+}]_{cyt}$ rise despite that $A\beta_{25-35}$ increases $[Ca^{2+}]_{cyt}$ in the same neurons and cells responded also to N-methyl D-aspartate (NMDA) and K^+ (Fig. 1D). In contrast to fibrils, $A\beta_{1-42}$ oligomers, at 500 nM, induce a large and sustained increase in $[Ca^{2+}]_{cyt}$ in most cells (Fig. 1E). The increases in $[Ca^{2+}]_{cyt}$ induced by $A\beta_{1-42}$ oligomers are heterogeneous showing different lags and kinetics and often $[Ca^{2+}]_{cyt}$ remain increased after washout of the peptide. The increase in $[Ca^{2+}]_{cyt}$ induced by $A\beta_{1-42}$ oligomers is also inhibited in medium lacking extracellular Ca^{2+} (Fig. 1F) and addition of extracellular Ca^{2+} restores the response. $A\beta_{25-35}$ and $A\beta_{1-42}$ oligomers increase $[Ca^{2+}]_{cyt}$ in 90±9 and 82±9% of the cells, respectively. The maximum $\Delta[Ca^{2+}]_{cyt}$ for responsive cells was 1290±247 nM for $A\beta_{25-35}$ and 1050±63 nM for $A\beta_{1-42}$ oligomers. In contrast, only 12±4% of the cells responded to $A\beta_{1-42}$ fibrils and the maximum $\Delta[Ca^{2+}]_{cyt}$ for responsive cells was 258±23 nM (data from 727 cells studied in 15 independent experiments). Most cells showing a Ca^{2+} response to $A\beta_{1-42}$ oligomers also respond to NMDA suggesting that responsive cells are neurons rather than glia (Fig. 1F). To confirm this finding we identified responsive cells by means of two-fold immunocytochemistry against neurons and glia in the same microscopic field used for Ca^{2+} imaging. Fig. 1G shows a representative example in which cells were identified by immunostaining (red, glia; green, neurons; blue, nuclei) after Ca^{2+} imaging. Neurons but not glia undergo increases in $[Ca^{2+}]_{cyt}$ after presentation of $A\beta_{1-42}$ oligomers.

We have tested also the effects of $A\beta_{1-42}$ oligomers on $[Ca^{2+}]_{cyt}$ in cortical and hippocampal neurons. Fig. 2 shows that $A\beta_{1-42}$ oligomers (500 nM) induce very large increases in $[Ca^{2+}]_{cyt}$ in both cortical (Fig. 2A) and hippocampal neurons (Fig. 2B). Most cells present in the microscopic fields responded to $A\beta_{1-42}$ oligomers in both cortical (83±9%, n = 218 cells, 3 experiments) and hippocampal (87±2%, n = 149 cells, 3 experiments) cells. In addition, the same cells that responded to $A\beta_{1-42}$ oligomers also responded to NMDA suggesting that responsive cells are neurons rather than glia (Fig. 2). Taken together, the results indicate that $A\beta_{25-35}$ and $A\beta_{1-42}$ oligomers promote massive Ca^{2+} influx in GT1 neural cells, cerebellar granules as well as cortical and hippocampal neurons. In contrast, $A\beta_{1-42}$ fibrils, at concentrations that are equally toxic than oligomers, produce no rises in $[Ca^{2+}]_{cyt}$ indicating that the mechanism of neurotoxicity may be different as proposed previously [21].

Aβ oligomers induce mitochondrial Ca^{2+} overload

We studied next whether Aβ peptides promote also mitochondrial Ca^{2+} uptake. We and others have reported previously that $[Ca^{2+}]_{mit}$ may rise substantially and that most $[Ca^{2+}]_{mit}$ measurements have been largely underestimated due to the use of non-targeted probes with high affinity for Ca^{2+} [22–24]. Accordingly, we used bioluminescence imaging of neurons expressing a low-affinity aequorin targeted to mitochondria developed previously to monitor the high-$[Ca^{2+}]$ levels inside the endoplasmic reticulum (ER, 24). This probe contains also GFP to select transfected neurons for bioluminescence imaging (mGA, 25). Fig. 3 shows the fluorescence (GFP, top) and bioluminescence (aequorin, bottom) images of cerebellar granule cells transfected with the mGA plasmid. We reported previously that stimulation of sympathetic

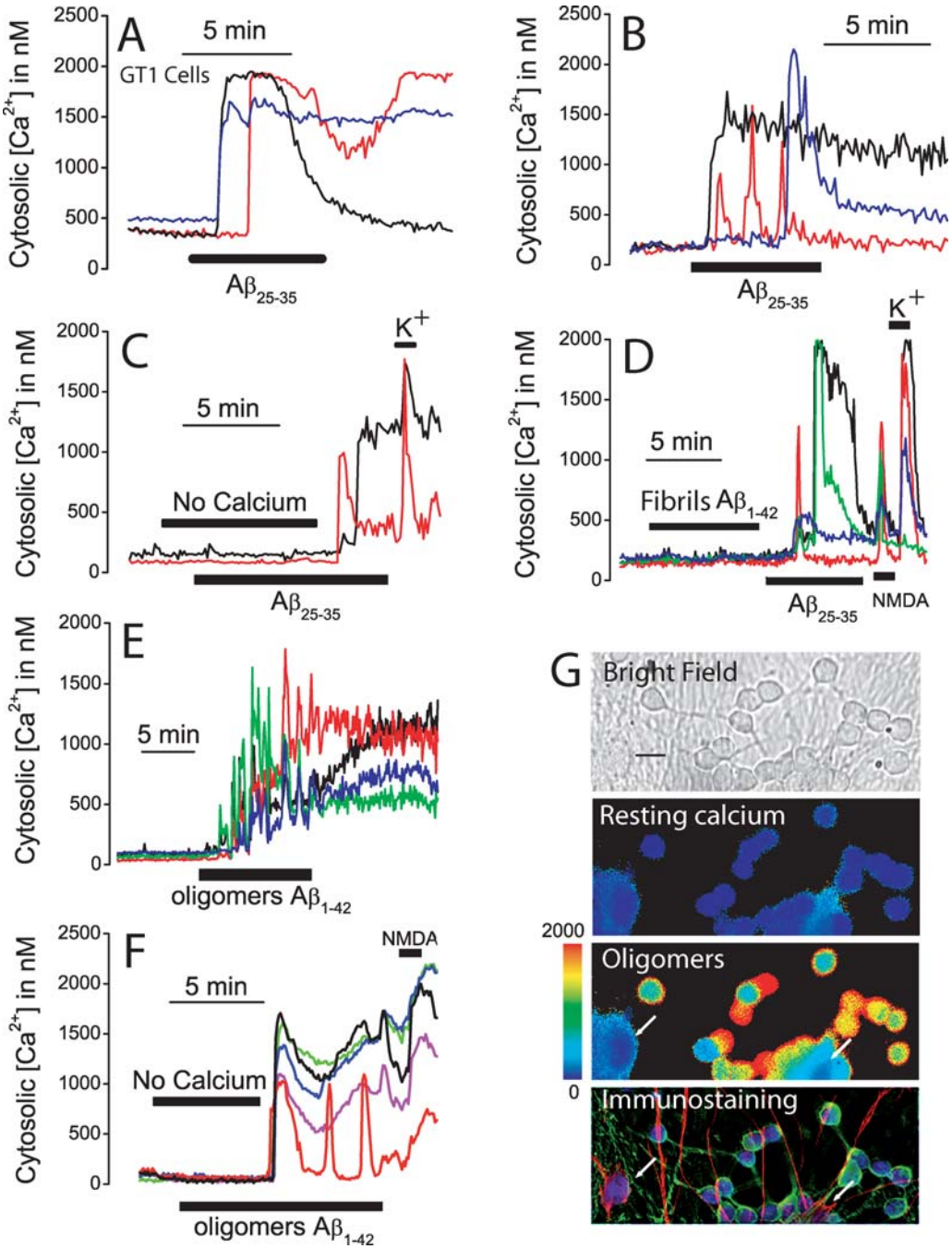

Figure 1. $A\beta_{1-42}$ oligomers but not fibrils induce Ca^{2+} influx in neurons. *A–B*. GT1 neural cells and cerebellar granule cells were loaded with fura2/AM and subjected to calcium imaging. Traces show the effects of $A\beta_{25-35}$ (20 μM) on $[Ca^{2+}]_{cyt}$ in three representative GT1 neural cells (*A*) and cerebellar granule cells (*B*). Data representative of 141–233 cells studied in 4 and 3 independent experiments, respectively. *C*. The increase in $[Ca^{2+}]_{cyt}$ induced by $A\beta_{25-35}$ (20 μM) in cerebellar granule cells is abolished in medium lacking extracellular Ca^{2+} (No calcium). Addition of normal medium containing 1 mM Ca^{2+} restored the response to $A\beta_{25-35}$. High K^+ medium (150 mM K^+) induced a further increase in $[Ca^{2+}]_{cyt}$. Traces correspond to two individual cells representative of n = 98 cells, 2 experiments). *D*. $A\beta_{1-42}$ fibrils (2 μM) induced little or no $[Ca^{2+}]_{cyt}$ increase in cerebellar granule cells. The same cells responded $A\beta_{25-35}$ (20 μM), N-methyl D-aspartate (100 μM NMDA) and high K^+ medium (150 mM K^+). (Traces correspond to four individual cells representative of n = 90 cells 3 experiments). *E*. $A\beta_{1-42}$ oligomers (500 nM) induced a large and sustained increase in $[Ca^{2+}]_{cyt}$ in cerebellar granules cells. Traces correspond to four individual cells representative of n = 404 cells 5 experiments). *F*. The effects of $A\beta_{1-42}$ oligomers (500 nM) are inhibited in medium lacking extracellular Ca^{2+} (No calcium). Perfusion of medium containing Ca^{2+} restored the response to Aβ oligomers. Cells also responded to 100 μM NMDA (recordings correspond to 5 individual cells representative of n = 283 cells, 3 experiments). *G*. Cerebellar granule cells were subjected to calcium imaging and then identified by double immunocytochemistry. Pictures show a bright field image (scale bar represents 10 μm) and $[Ca^{2+}]_{cyt}$ levels before (resting calcium) and after treatment with $A\beta_{1-42}$ oligomers (oligomers) coded in pseudocolor (pseudocolor bar from 0 to 2000 nM shown at left) and immunostaining of the cells. Glial cells (arrows) are coded in red, neurons are coded in green and nuclei are coded in blue. Only neurons responded to Aβ oligomers with a rise in $[Ca^{2+}]_{cyt}$. Data representative of 249 cells, 3 experiments.
doi:10.1371/journal.pone.0002718.g001

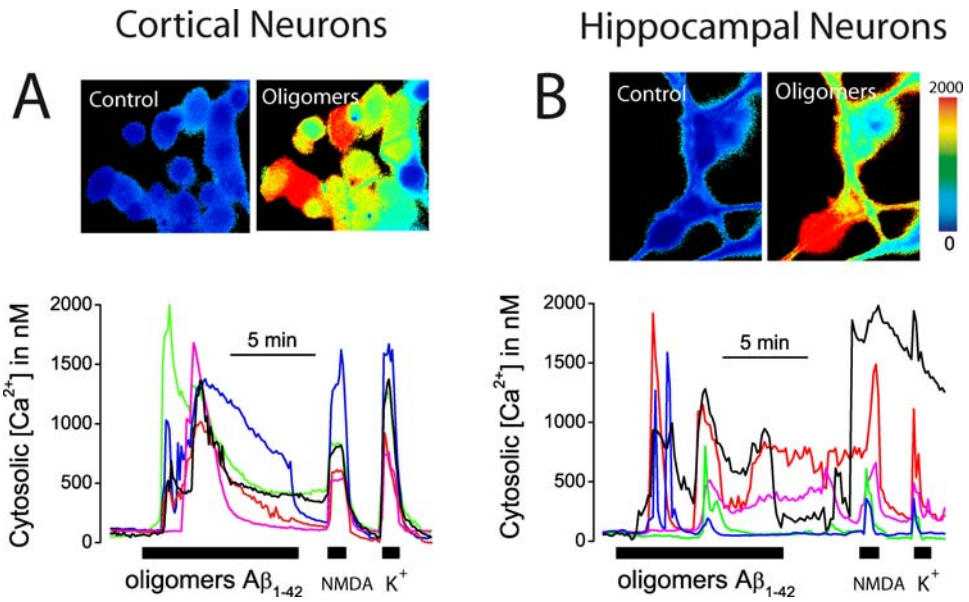

Figure 2. $A\beta_{1-42}$ oligomers induce $[Ca^{2+}]_{cyt}$ increases in cortical and hippocampal neurons. Pictures show pseudocolor images of $[Ca^{2+}]_{cyt}$ before (control) and after (oligomers) perfusion with 500 nM $A\beta_{1-42}$ oligomers in cortical (A) and hippocampal (B) neurons loaded with fura4F. Pseudocolor scale shown at right. Traces are recordings of $[Ca^{2+}]_{cyt}$ in 5 representative cortical (A) and hippocampal (B) neurons during stimulation with $A\beta_{1-42}$ oligomers. Cells responding to $A\beta_{1-42}$ oligomers also responded to 100 μM NMDA and 150 mM K^+. Data are representative of n = 218 cortical cells and n = 149 hippocampal cells studied in at least 3 independent experiments for each brain area.
doi:10.1371/journal.pone.0002718.g002

neurons and other excitable cells expressing low-affinity, mitochondria-targeted aequorin with high K^+ medium (to open voltage-gated Ca^{2+} channels) release typically 5–10% of photonic emissions (expressed as the % of remaining counts) that, when calibrated, reported increases in $[Ca^{2+}]_{mit}$ of about 100–300 μM. In addition, these $[Ca^{2+}]_{mit}$ rises were limited to a pool of mitochondria close to sites of Ca^{2+} entry and release [16,23,25]. We found that, in marked contrast, $A\beta_{25-35}$ (Fig. 3A) and $A\beta_{1-42}$ oligomers (Fig. 3B) released nearly all photonic emissions in responsive neurons which, after calibration, reported an average increase in $[Ca^{2+}]_{mit}$ close to the mM level. Like the rises in $[Ca^{2+}]_{cyt}$, the increases in $[Ca^{2+}]_{mit}$ were heterogeneous in terms of lag, size and kinetics. On average, $A\beta_{25-35}$ induced a $[Ca^{2+}]_{mit}$ increase in 67±3% of the cells (mean±SEM, 1008±250 μM, 37 cells, 3 experiments) whereas 62±10% of the neurons responded to $A\beta_{1-42}$ oligomers with a large increase in $[Ca^{2+}]_{mit}$ (960±200 μM, 36 cells, 3 experiments). In contrast, $A\beta_{1-42}$ fibrils failed to induce any increase in $[Ca^{2+}]_{mit}$ (n = 3 experiments, data not shown) consistently with the lack of effects on $[Ca^{2+}]_{cyt}$. The rises in $[Ca^{2+}]_{mit}$ induced by $A\beta_{25-35}$ and $A\beta_{1-42}$ oligomers in intact neurons were similar to the increase in $[Ca^{2+}]_{mit}$ induced by perfusing permeabilized neurons with intracellular medium (see Methods) containing 5 μM Ca^{2+}. This rise was prevented by the mitochondrial Ca^{2+} uniporter blocker ruthenium red and by collapsing the mitochondrial potential ($\Delta\Psi$) with 10 μM FCCP (data not shown). $A\beta_{25-35}$ induced a similar large increase in both $[Ca^{2+}]_{cyt}$ and $[Ca^{2+}]_{mit}$ in GT1 neural cells (data not shown). We tested also the effects of $A\beta_{1-42}$ on $[Ca^{2+}]_{mit}$ in cortical neurons. $A\beta_{1-42}$ oligomers also induced large $[Ca^{2+}]_{mit}$ increases in a large population (75±5%, n = 91 cells, 6 experiments) of cortical neurons (Fig. 3C). In the responsive cortical neurons, the average rise in $[Ca^{2+}]_{mit}$ was 1099±93 μM (mean±SEM). Taken together, these results show that $A\beta_{25-35}$ and $A\beta_{1-42}$ oligomers, but not fibrils, induce a large and sustained entry of Ca^{2+} through the plasma membrane followed by mitochondrial Ca^{2+} overload in all neuronal cell models tested here. We asked next whether $A\beta_{1-42}$ oligomers induce apoptosis and cell death and if so, for the possible role of mitochondrial Ca^{2+} overload in that process.

Aβ induces apoptosis and cell death in neurons

Since mitochondrial Ca^{2+} overload may promote opening of the mitochondrial permeability transition pore (mPTP) and the intrinsic pathway to apoptosis [26,27], we have studied whether exogenously added $A\beta_{1-42}$ oligomers promote apoptotic processes in cerebellar granule cells. For assessing mPTP opening we used the calcein/Co^{2+} method [28]. Calcein fluorescence distributes in both cytosol and mitochondria but only cytosolic calcein is quenched by Co^{2+}. Opening of mPTP promotes mitochondrial calcein quenching. Fig 4A shows that $A\beta_{1-42}$ oligomers induce quenching of mitochondrial calcein fluorescence in cells loaded with calcein and $CoCl_2$ and this effect is prevented by cyclosporin A, a mPTP blocker. $A\beta_{1-42}$ oligomers also promote release of cytochrome c (Fig. 4B), apoptosis (Fig. 4C) and cell death (Fig. 4D) as shown by conventional immunofluorescence against cytochrome c, TUNEL assay and dye exclusion studies, respectively. Cell death induced by Aβ oligomers is inhibited by cyclosporin A (Fig. 4D). $A\beta_{25-35}$ also induces apoptosis and cell death in cerebellar granule cells (Figure S2). These results indicate that $A\beta_{1-42}$ oligomers promote a mitochondrial pathway to apoptosis. These effects are quite well mimicked by the toxic fragment $A\beta_{25-35}$, although at far larger concentrations.

Mitochondrial Ca^{2+} overload contributes to Aβ-induced apoptosis

We asked next for the contribution of mitochondrial Ca^{2+} overload to the apoptosis induced by $A\beta_{1-42}$ oligomers and $A\beta_{25-35}$. For this end we have studied whether inhibition of mitochondrial Ca^{2+} uptake prevents Aβ oligomers-induced apoptosis or not. Ca^{2+} uptake by mitochondria depends exponentially on $\Delta\Psi$, a huge driving force of −180 mV built

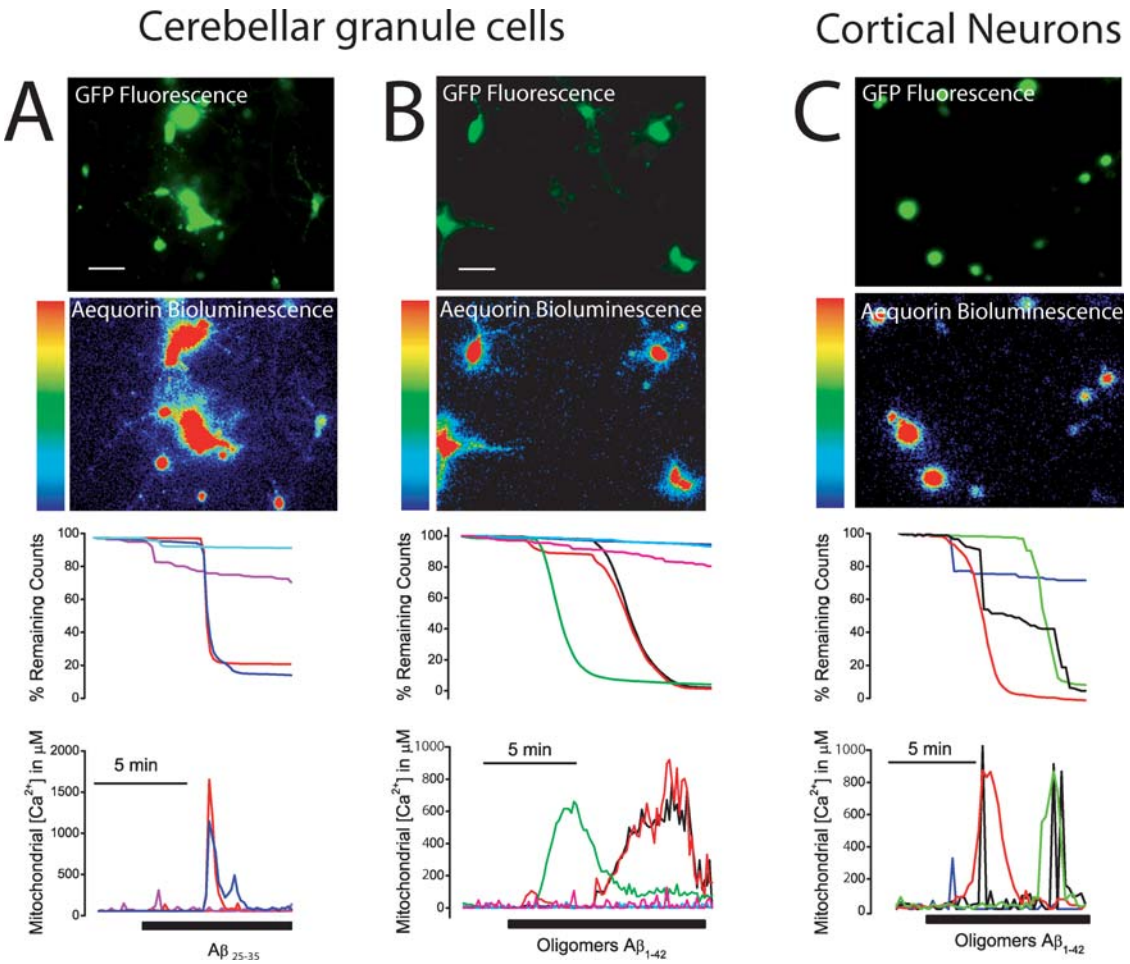

Figure 3. $A\beta_{1-42}$ oligomers induce mitochondrial Ca^{2+} overload. Cerebellar granule cells and cortical neurons were transfected with the low-affinity, mitochondria-targeted aequorin fused to GFP, incubated with 1 µM n coelenterazine and subjected to bioluminescence imaging of $[Ca^{2+}]_{mit}$. Pictures show the fluorescence (top, GFP fluorescence) and accumulated photonic emissions (bottom, Aequorin Bioluminescence) images of representative microscopic fields (scale bar represents 10 µm). Luminescence intensity is coded in pseudocolor (1 to 32 photons per pixel). Traces show the effects of $A\beta_{25-35}$ (20 µM, A) and $A\beta_{1-42}$ oligomers (500 nM, B) on % of remaining counts (top traces) and calibrated $[Ca^{2+}]_{mit}$ (bottom traces) in individual, representative cerebellar granule cells (A,B) and cortical neurons (C). Data are representative of 37, 36 and 68 individual cells studied in 3 independent experiments, respectively.
doi:10.1371/journal.pone.0002718.g003

upon the respiratory chain. We have reported recently that a small mitochondrial depolarization is enough to prevent largely mitochondrial Ca^{2+} uptake [29,30]. Accordingly, we studied the effects of a small mitochondrial depolarization using low concentrations of the mitochondrial uncoupler FCCP. To assess the effects of this treatment on $\Delta\Psi$ we used TMRM, a cationic dye that accumulates in mitochondria according to $\Delta\Psi$ and is considered one of the most sensitive $\Delta\Psi$ probes available [31]. Confocal images of cerebellar granule cells co-stained with mitotracker green and TMRM show the mitochondrial localization of the probe (Fig. 5A). Addition of FCCP decreases TMRM fluorescence in a dose–dependent manner consistent with a mitochondrial depolarization (Fig. 5B). At 100 nM, FCCP decreases TMRM fluorescence by about 25% relative to the total fluorescence decrease induced by 10 µM FCCP. According to our previous report [30], we estimate that such a decrease in TMRM fluorescence induced by 100 nM FCCP corresponds to a loss of $\Delta\Psi$ of about 10–20 mV; whereas at 10 µM, FCCP decreases fully TMRM fluorescence consistently with a collapse of $\Delta\Psi$ (Fig. 5C). Similar results were found in GT1 neural cells (data not shown). Strong plasma membrane depolarization with high K^+ medium (50 mM) did not affect TMRM fluorescence excluding the possibility that TMRM is reporting changes in the plasma membrane potential (data not shown). Next, we studied the effects of such an small mitochondrial depolarization on mitochondrial Ca^{2+} uptake. We found that FCCP, at 100 nM, prevents the increase in $[Ca^{2+}]_{mit}$ induced by $A\beta_{1-42}$ oligomers (Fig. 5D). Specifically, 100 nM FCCP inhibits by 78±4% the $[Ca^{2+}]_{mit}$ increase induced by $A\beta_{1-42}$ oligomers (n = 21 cells, 3 experiments). FCCP also inhibited the rise in $[Ca^{2+}]_{mit}$ induced by $A\beta_{25-35}$ (Figure S3A). Specifically, 100 nM FCCP inhibits by 82±5% the $[Ca^{2+}]_{mit}$ increase induced by $A\beta_{25-35}$ (17 cells studied, 3 experiments). This effect is not due to inhibition of Ca^{2+} entry through the plasma membrane since 100 nM FCCP does not prevent at all the increase in $[Ca^{2+}]_{cyt}$ induced by $A\beta_{1-42}$ oligomers (Fig. 5E) or $A\beta_{25-35}$ (Figure S3B).

Once that conditions are established for specific inhibition of mitochondrial Ca^{2+} uptake, we addressed the contribution of mitochondrial Ca^{2+} overload to the cell death induced by $A\beta_{1-42}$ oligomers. For this end, we studied the effects of 100 nM FCCP on $A\beta_{1-42}$ oligomers-induced cytochrome c release and cell death. We find that FCCP at 100 nM prevents both cytochrome c release

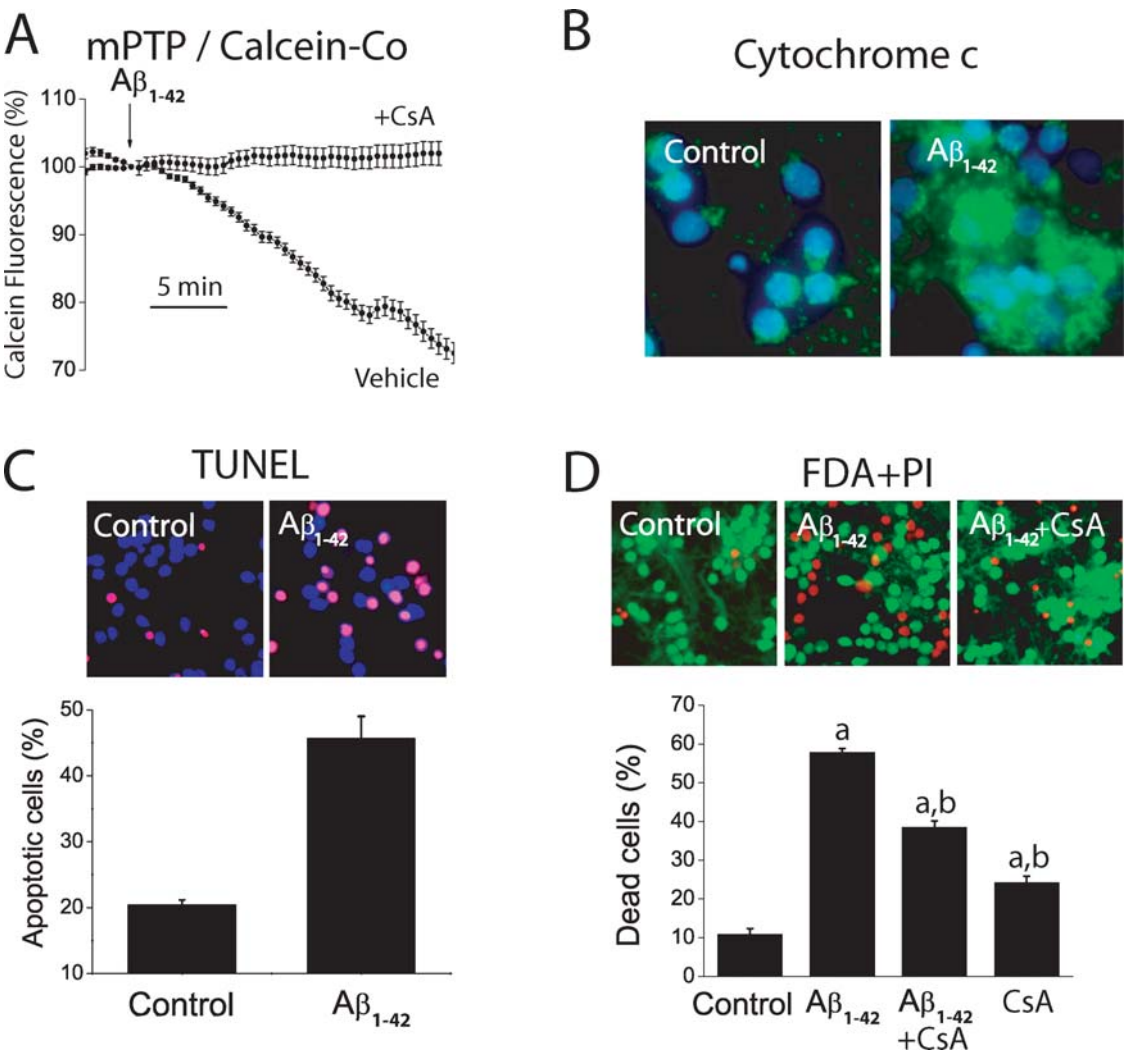

Figure 4. $A\beta_{1-42}$ oligomers induce mPTP opening, cytochrome c release, apoptosis and cell death. *A*. Mitochondrial permeability transition was assessed directly by the calcein/Co^{2+} method. Cerebellar granule cells were loaded with calcein/AM 1 μM and $CoCl_2$ 1 mM for 15 min at 37°C and calcein fluorescence quenching was imaged. Traces correspond to mean±SEM fluorescence records normalized to the value before the addition of oligomeric $A\beta_{1-42}$ (500 nM) in responsive cells (n = 16 cells, vehicle) or in cyclosporin (1 μM) treated cells. Representative of 3 experiments. *B*. Location of cytochrome c was assessed by immunofluorescence against cytochrome c. Cerebellar granule cells were cultured for 72 h in vehicle or 500 nM $A\beta_{1-42}$ oligomers. Blue colors show nuclei stained with DAPI. Green colors show location of cytochrome c. Control cells show punctate distribution of cytochrome c. Aβ oligomers-treated cells show a more diffuse location of cytochrome c due to release of cytochrome c from mitochondria. Representative of 3 independent experiments. Scale bar represents 10 μm. *C*. Cerebellar granule cells were cultured for 72 h in vehicle or $A\beta_{1-42}$ oligomers (500 nM) and apoptosis was tested by TUNEL assay. Pictures show nuclei (blue) and apoptotic cells (purple). Bars show % of apoptotic cells. (n = 3; *p<0 05). Scale bar represents 10 μm. *D*. Cerebellar granule cells were cultured for 72 h with vehicle (control) or $A\beta_{1-42}$ oligomers (500 nM) and cell death was assessed by staining with FDA (green living cells) and PI (red dead cells, scale bar represents 10 μm. Shown are also the effects cyclosporin A (1 μM) on $A\beta_{1-42}$ oligomers-induced death in cerebellar granule cells (n = 3; [a]p<0 05 vs control; [b]p<0 05 vs $A\beta_{1-42}$). Representative of 3 independent experiments.
doi:10.1371/journal.pone.0002718.g004

induced by both $A\beta_{1-42}$ oligomers (Fig. 5F,G) and $A\beta_{25-35}$ (Figure S3C,D). Consistently, we find that FCCP 100 nM inhibits cell death induced by both $A\beta_{25-35}$ in cerebellar granule cells (Fig. 5H) and GT1 cells (Fig. 5I). Finally, 100 nM FCCP also inhibits cell death induced by $A\beta_{1-42}$ oligomers in cerebellar granule cells (Fig. 5J). These results indicate that inhibition of mitochondrial Ca^{2+} overload by a partial mitochondrial depolarization protects against the neurotoxicity induced by $A\beta_{1-42}$ oligomers and $A\beta_{25-35}$.

It has been reported that mitochondrial Ca^{2+} overload during excitotoxicity may promote reactive oxygen species (ROS) production and contribute to neuron cell damage [32]. Accordingly, we also studied the effects of $A\beta_{1-42}$ oligomers on ROS production in cerebellar granule cells. Incubation of cerebellar granule cells with 500 nM $A\beta_{1-42}$ oligomers for 4 h elicited a clear increase in number of neurons strongly stained by the ROS probe CM-H2DCFDA. This effect was absent in cells incubated previously with 100 nM FCCP added here to prevent the $A\beta_{1-42}$ induced increase in $[Ca^{2+}]_{mit}$ (Figure S4). These results suggest that mitochondrial Ca^{2+} overload may contribute to ROS production induced by $A\beta_{1-42}$ oligomers.

NSAIDs depolarize mitochondria and inhibit mitochondrial Ca^{2+} uptake

The above results open the question on whether drugs preventing mitochondrial Ca^{2+} overload may or may not protect

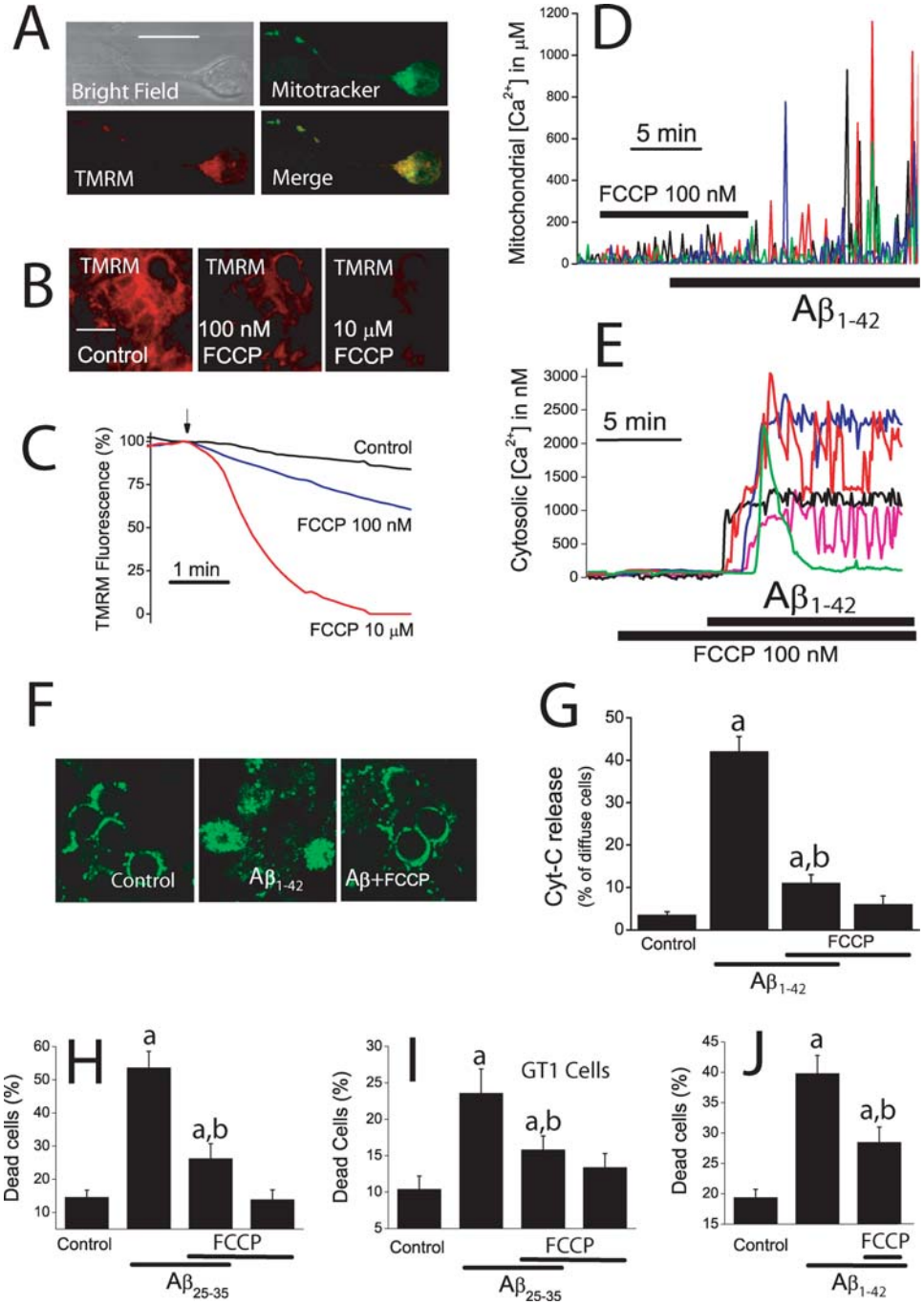

Figure 5. Mitochondrial Ca^{2+} uptake contributes to cell death induced by Aβ oligomers. *A*. Cerebellar granule cells were co-loaded with mitotracker green and TMRM 10 nM and washed. Double staining was assessed by confocal microscopy. Pictures show bright field mitotracker staining, TMRM staining and merge of mitotracker and TMRM staining. Images confirm the mitochondrial location of the TMRM probe. Scale bar represents 10 μm. *B*. Cells were loaded with TMRM 10 nM and mitochondrial depolarization was estimated by the decrease in TMRM fluorescence. Pictures show TMRM fluorescence images of cerebellar granule cells treated for 5 min with vehicle (control), 100 nM FCCP or 10 μM FCCP. Scale bar represents 10 μm. *C*. Traces show fluorescence recordings of cerebellar granule cells stained with 10 nM TMRM. Fluorescence values from individual cells were normalized to the value before addition (arrow) of either vehicle or FCCP and averaged. Each trace is the mean of 45–67 cells and representative of at least 3 independent experiments. *D*. Cerebellar granule cells expressing mGA were subjected to bioluminescence for $[Ca^{2+}]_{mit}$ measurements. FCCP 100 nM inhibits the increase in $[Ca^{2+}]_{mit}$ induced by $A\beta_{1-42}$ oligomers (500 nM, 21 cells, 3 experiments). After washout of FCCP, $A\beta_{1-42}$ oligomers were able to increase $[Ca^{2+}]_{mit}$. *E*. Cerebellar granule cells were loaded with fura2/AM and subjected to fluorescence imaging for $[Ca^{2+}]_{cyt}$ measurements. FCCP 100 nM failed to inhibit the increase in $[Ca^{2+}]_{cyt}$ induced by $A\beta_{1-42}$ oligomers (500 nM) (n = 78 cells, 3 experiments). *F*. Immunofluorescence against cytochrome c was assessed by confocal microscopy in cerebellar granule cells treated with vehicle (Control), $A\beta_{1-42}$ oligomers 500 nM (Aβ) and $A\beta_{1-42}$ oligomers+FCCP 100 nM (Aβ+FCCP) for 72 h. $A\beta_{1-42}$ oligomers promote diffusion of cytochrome c that otherwise shows a punctate staining. 100 nM FCCP prevented diffusion of cytochrome C. Scale bar represents 10 μm. *G*. Bars show % of cells showing diffuse staining for cytochrome c (reflecting cytochrome c release). $A\beta_{1-42}$ oligomers (500 nM) increase the % of cells showing diffuse staining, an effect inhibited by FCCP 100 nM. *H–J*. FCCP 100 nM inhibits cell death induced by 20 μM $A\beta_{25-35}$ in cerebellar cells (H) and GT1 cells (I) and by 500 nM $A\beta_{1-42}$ oligomers in cerebellar granule cells (J) as assessed by dye exclusion studies. [a]$p<0$ 05 *vs*. control; All data are mean±SEM of 3 independent experiments.

doi:10.1371/journal.pone.0002718.g005

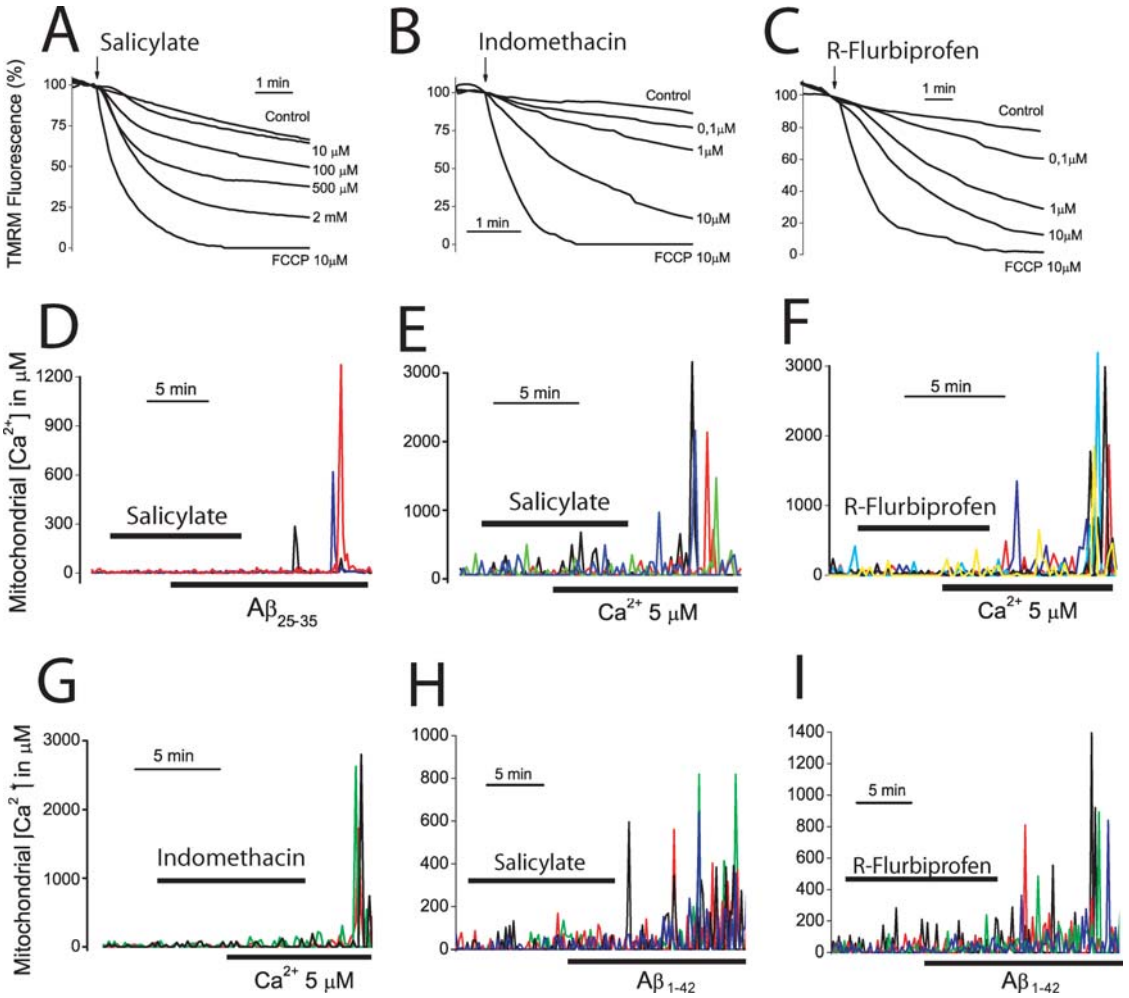

Figure 6. NSAIDs depolarize mitochondria and inhibit mitochondrial Ca^{2+} uptake. *A–C*. Cerebellar granule cells were stained with 10 nM TMRE and subjected to fluorescence microscopy for monitoring changes in mitochondrial potential. Each trace correspond to averaged, normalized fluorescence values of 34–42 cells treated (arrow) with vehicle (control) or different concentrations of salicylate (A, 10 μM to 2 mM), indomethacin (B, 0.1 to 10 μM), R-flurbiprofen (C, 0.1 to 10 μM). FCCP 10 μM was also added to compare with conditions of collapse of the mitochondrial potential. Each series of recordings is representative of at least 3 experiments. *D–F*. Cerebellar granule cells were transfected with the mGA plasmid and subjected to bioluminescence imaging for monitoring $[Ca^{2+}]_{mit}$. Salicylate (D, 100 μM) inhibits the $[Ca^{2+}]_{mit}$ induced by $A\beta_{25-35}$ (20 μM, n = 43 cells, 3 experiments). In some experiments, cerebellar granule cells expressing mGA were permeabilized in intracellular medium containing 200 nM Ca^{2+} (see methods) and treated with salicylate 100 μM (E), R-flurbiprofen 1 μM (F) or indomethacin 1 μM (G) before being stimulated with the same intracellular medium containing 5 μM Ca^{2+} to stimulate mitochondrial Ca^{2+} uptake (Data from 188 cells studied in 6 independent experiments). *H,I*. Salicylate 100 μM and R-flurbiprofen 1 μM also inhibits the increase in $[Ca^{2+}]_{mit}$ induced by $A\beta_{1-42}$ oligomers (500 nM). Data from n = 35 and 30 cells respectively, studied in 3 independent experiments for each drug.
doi:10.1371/journal.pone.0002718.g006

against $A\beta_{1-42}$ oligomers and $A\beta_{25-35}$. We have shown recently that salicylate, the mayor aspirin metabolite, depolarizes mitochondria and inhibit mitochondrial Ca^{2+} uptake in human colon carcinoma cells at low, therapeutic concentrations [29,30]. Accordingly, we asked whether salicylate and other carboxylic NSAIDs depolarize mitochondria and inhibit mitochondrial Ca^{2+} uptake in cerebellar granule cells. Figs. 6A–C show that salicylate, indomethacin and R-flurbiprofen decrease TMRM fluorescence in a dose-dependent manner in intact neurons consistent with a partial mitochondrial depolarization. Shown are also the effects of 10 μM FCCP (lowest traces in each panel in Figs. 6A–C), a concentration that collapses the mitochondrial potential. A similar mitochondrial depolarization than that provoked by 100 nM FCCP (Fig. 5C) was elicited by 100 μM salicylate and by 0,1–1 μM of the remaining NSAIDs including R-flurbiprofen, an enantiomer derivative lacking anti-inflammatory activity. Next, we studied the effects of NSAIDs on mitochondrial Ca^{2+} uptake. We find that salicylate, indomethacin and R-flurbiprofen inhibit the mitochondrial Ca^{2+} overload induced by either $A\beta_{25-35}$ in intact cells or by 5 μM Ca^{2+} in permeabilized neurons (Fig. 6D–G). Specifically, salicylate, at 100 μM, decreased by 78±4% the $A\beta_{25-35}$-induced $[Ca^{2+}]_{mit}$ rise in intact cells and by 77±6% the Ca^{2+}-induced rise in $[Ca^{2+}]_{mit}$ in permeabilized neurons (data from 157 cells studied in 4 independent experiments). Indomethacin, sulindac sulfide and R-flurbiprofen, all tested at 1 μM, inhibited by 77±3, 86±4 and 68±1%, respectively, the Ca^{2+}-induced rise in $[Ca^{2+}]_{mit}$ in permeabilized neurons (data from 188 cells studied in 6 independent experiments). Salicylate and R-flurbiprofen also prevented the $[Ca^{2+}]_{mit}$ rise induced by $A\beta_{1-42}$ oligomers (Fig. 6H,I). Specifically, salicylate at 100 μM and R-flurbiprofen at 1 μM inhibited by 77±4% and 85±3%, respectively (mean±‴ SEM) the $[Ca^{2+}]_{mit}$ increase induced by $A\beta_{1-42}$ oligomers (n = 35

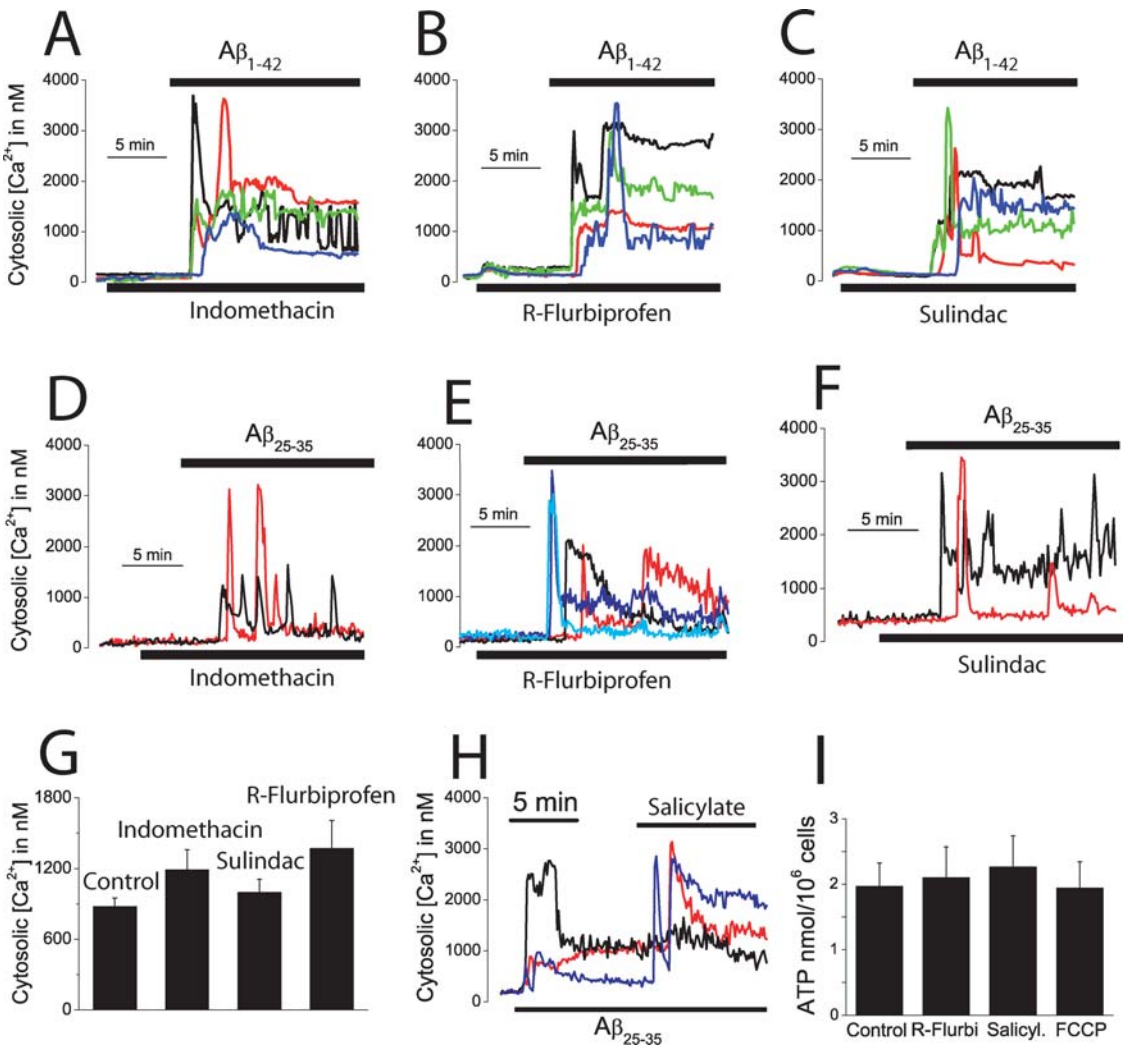

Figure 7. NSAIDs do not prevent the increase in $[Ca^{2+}]_{cyt}$ induced by $A\beta_{1-42}$ oligomers or affect cell ATP levels. *A–C*, cerebellar granule cells were loaded with fura4F/AM and subjected to calcium imaging to test the effects of several NSAIDs on the increases in $[Ca^{2+}]_{cyt}$ induced by $A\beta_{1-42}$ oligomers. Neither indomethacin (A), R-flurbiprofen (B) or sulindac sulfide (C), all tested at 1 μM, inhibit the increase in $[Ca^{2+}]_{cyt}$ induced by $A\beta_{1-42}$ oligomers. Data corresponds to 76–120 cells, corresponding to at least 2 experiments. *D–G*, indomethacin, R-flurbiprofen or sulindac sulfide (all tested at 1 μM) neither inhibit the increase in $[Ca^{2+}]_{cyt}$ induced by $A\beta_{25-35}$. Shown are representative recordings of individual cells (46–90 cells studied in 3 independent experiments respectively). *G*. The maximum increase in $[Ca^{2+}]_{cyt}$ induced by $A\beta_{25-35}$ (20 μM) was calculated for cells treated with vehicle (control) or the above NSAIDs ($p>0,05$; $n=3$). *H*. Salicylate 100 μM increased $[Ca^{2+}]_{cyt}$ further in cells treated with $A\beta_{25-35}$ (20 μM). Representative recordings of 164 cells studied in 3 independent experiments. *I*. Cerebellar granule cells were treated with vehicle, 1 μM R-flurbiprofen, 100 μM salicylate and 100 nM FCCP for 72 h and cell ATP levels were measured. None of the treatments decreases significantly cell ATP levels ($p>0,05$; $n=3$).
doi:10.1371/journal.pone.0002718.g007

and 30 cells, respectively, studied in 3 independent experiments for each drug). These results indicate that NSAIDs inhibit mitochondrial Ca^{2+} uptake induced by $A\beta_{1-42}$ oligomers and $A\beta_{25-35}$ in intact cells and by high Ca^{2+} in permeabilized cells. In addition, they suggest that this effect is probably secondary to mitochondrial depolarization and therefore, inhibition of the driving force for Ca^{2+} uptake through the mitochondrial Ca^{2+} uniporter, rather than inhibition of Ca^{2+} entry through the plasma membrane. To support further this view we assessed the effects of NSAIDs on the increases in $[Ca^{2+}]_{cyt}$ induced by $A\beta_{1-42}$ oligomers and $A\beta_{25-35}$. None of the NSAIDs tested including indomethacin, R-flurbiprofen and sulindac sulfide, all tested at 1 μM, produce any change in resting $[Ca^{2+}]_{cyt}$ or prevent the increase in $[Ca^{2+}]_{cyt}$ induced by $A\beta_{1-42}$ oligomers (Fig. 7A–C) or $A\beta_{25-35}$ (Fig. 7D–G). Moreover, addition of NSAID (salicylate) over the increased $[Ca^{2+}]_{cyt}$ induced by $A\beta_{25-35}$ not only failed to decrease the level of $[Ca^{2+}]_{cyt}$ but rather increased it (Fig. 7H), an effect that can be explained by mitochondrial uncoupling and release of Ca^{2+} from preloaded mitochondria [33]. Because a large mitochondrial depolarization may affect cell metabolism, we tested whether or not the small depolarization induced by low concentrations of FCCP and NSAIDs may affect cell ATP levels. Fig. 7I shows that neither FCCP (100 nM), salicylate (100 μM) or R-flurbiprofen (1 μM) decrease the cell ATP levels in cerebellar granule cells. These results indicate that NSAIDs, at low μM concentrations, inhibit specifically mitochondrial Ca^{2+} uptake without preventing entry of Ca^{2+} through the plasma membrane and this effect is most likely mediated by a partial mitochondrial depolarization. We recently adapted an algorithm to convert TMR fluorescence values into estimated $\Delta\Psi$ expressed in mV [30]. According to that algorithm, we estimate that the loss of $\Delta\Psi$ induced by the low FCCP and NSAIDs concentrations used here is only 10–20 mV.

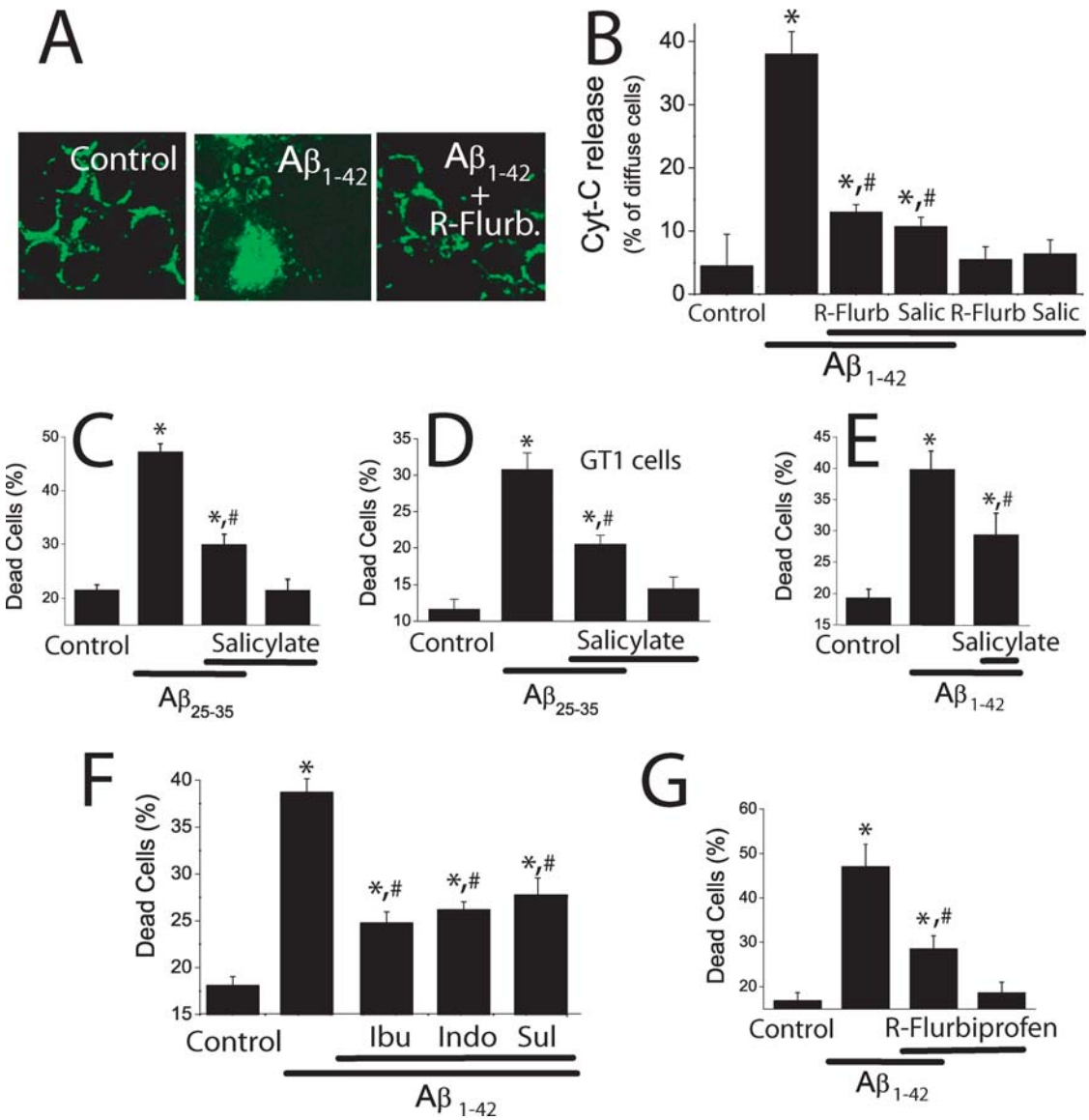

Figure 8. NSAIDs inhibit cytochrome c release and cell death induced by $A\beta_{1-42}$ oligomers. *A,B*. Cerebellar granule cells were treated with $A\beta_{1-42}$ (500 nM) for 72 h with or without 1 μM R-flurbiprofen or 100 μM salicylate and fixed for analysis of cytochrome c location using confocal microscopy. *A*. Control cells showed a punctate distribution of cytochrome c. Scale bar represents 10 μm. $A\beta_{1-42}$ oligomers-treated cells show a more diffuse pattern of cytochrome c whereas cells treated with $A\beta_{1-42}$ oligomers plus R-flurbiprofen show a punctate pattern similar to control cells. *B*. Bars show the relative abundance (%) of cells showing diffuse immunostaining in control cells, cells treated with $A\beta_{1-42}$ oligomers and cells treated with $A\beta_{1-42}$ oligomers plus 1 μM R-flurbiprofen or 100 μM salicylate (B). *$p<0$ 05 vs control; #$p<0$ 05 vs Aβ; data from at least 3 independent experiments. Salicylate 100 μM inhibits cell death induced by $A\beta_{25-35}$ (20 μM) in cerebellar granule cells (C) and GT1 cells (D). Salicylate 100 μM also inhibits cell death induced by $A\beta_{1-42}$ oligomers (500 nM) in cerebellar granule cells (E). (*$p<0$ 05 vs control; #$p<0$ 05 vs Aβ. n = 3). *F*. Ibuprofen (Ibu), Indomethacin (Indo), and sulindac sulfide (Sul), all tested at 1 μM, inhibit cell death induced by $A\beta_{1-42}$ oligomers (500 nM) in cerebellar granule cells. *G*. R-Flurbiprofen 1 μM also inhibits cell death induced by $A\beta_{1-42}$ oligomers (500 nM). *$p<0$ 05 *vs*. control; #$p<0$ 05 *vs* Aβ. All data are representative of 3 experiments.

doi:10.1371/journal.pone.0002718.g008

This very small mitochondrial depolarization should not compromise cell metabolism as suggested by the lack of effects of these treatments on cell ATP levels.

NSAIDs prevent neuron cell death induced by $A\beta_{1-42}$ oligomers

To learn whether inhibition of mitochondrial Ca^{2+} uptake by NSAIDs prevents cell death induced by $A\beta_{1-42}$ oligomers, we have studied the effects of the same low NSAID concentrations on $A\beta_{1-42}$ oligomers-induced cytochrome c release and cell death. We found that 1 μM R-flurbiprofen and 100 μM salicylate prevent cytochrome c release induced by $A\beta_{1-42}$ oligomers (Fig. 8A,B). R-flurbiprofen and salicylate prevent also cytochrome c release induced by $A\beta_{25-35}$ (Figure S5A–C). In addition, we found that 100 μM salicylate inhibits cell death induced by $A\beta_{25-35}$ in both cerebellar granule cells (Fig. 8C) and GT1 cells (Fig. 8D). Salicylate also inhibits cell death induced by $A\beta_{1-42}$ oligomers in cerebellar granule cells (Fig. 8E). Moreover, we found that 1 μM of either ibuprofen, indomethacin and sulindac sulfide prevented

cerebellar granule cell death induced by $A\beta_{1–42}$ oligomers (Fig. 8F) and $A\beta_{25–35}$ (Figure S5D). R-flurbiprofen prevented cell death induced by either $A\beta_{1–42}$ oligomers (Fig. 8G). In addition, R-flurbiprofen prevented cell death induced by $A\beta_{25–35}$ to the same extent than the S enantiomer (Figure S5E). Thus, NSAIDs inhibit cytochrome c release and cell death induced by either $A\beta_{1–42}$ and $A\beta_{25–35}$ at the same low concentrations that depolarize partially mitochondria and inhibit mitochondrial Ca^{2+} overload. Finally, we found that 1 μM R-flurbiprofen, like 100 nM FCCP, also inhibits ROS production induced by $A\beta_{1–42}$ oligomers (Figure S4).

Discussion

We show here that $A\beta_{1–42}$ oligomers, the assembly state that correlates best with brain damage and cognitive deficits in AD [13,14], but not Aβ fibrils, promote massive entry of Ca^{2+} into GT1 neural cells and cerebellar granule neurons but not glia. This view is supported by the finding that cells responding to $A\beta_{1–42}$ oligomers also respond to NMDA and by immunocytochemical identification of responsive cells. $A\beta_{1–42}$ oligomers, but not fibrils, also induced large increases in $[Ca^{2+}]_{cyt}$ in cortical and hippocampal neurons. These results agree with those recently reported [34] showing that $A\beta_{1–42}$ oligomers but not monomers or fibrils increased $[Ca^{2+}]_{cyt}$ in a human neuroblastoma cell line. The results suggest that the mechanism of neurotoxicity by fibrils and oligomers may be different as previously proposed [21]. The effects of $A\beta_{1–42}$ oligomers are quite well reproduced by the toxic fragment $A\beta_{25–35}$ although at 40-fold larger concentrations. The increases in $[Ca^{2+}]_{cyt}$ induced by $A\beta_{1–42}$ oligomers and the toxic fragment $A\beta_{25–35}$ can be attributed to enhanced entry of extracellular Ca^{2+} through the plasma membrane rather than release from intracellular Ca^{2+} stores as they were entirely prevented by removal of extracellular Ca^{2+}. The route for this enhanced Ca^{2+} influx is not solved yet but candidate mechanisms may include plasma membrane permeabilization [34], formation of the so-called amyloid channels [35,36] and/or activation of NMDA receptors [37]. Neither $A\beta_{25–35}$ or $A\beta_{1–42}$ oligomers induced parallel decreases in fura2 fluorescence excited at 340 and 380 nm (data not shown) suggesting that the rises in $[Ca^{2+}]_{cyt}$ are not due to membrane permeabilization. It has been shown previously that the increases in $[Ca^{2+}]_{cyt}$ induced by Aβ species can be prevented by the NMDA receptor open channel blocker memantine [37] and specific amyloid channel blockers [36] suggesting that both NMDA receptors and amyloid channels might be involved. In any case, the massive entry of Ca^{2+} induced by $A\beta_{1–42}$ oligomers promotes mitochondrial Ca^{2+} overload as shown directly by bioluminescence imaging of neurons expressing a low-affinity aequorin targeted to mitochondria. This probe was originally developed to monitor the high $[Ca^{2+}]$ inside the endoplasmic reticulum that reach the mM range in resting conditions [24]. Using this probe, we and others have shown previously that $[Ca^{2+}]_{mit}$ may reach several hundred μM upon stimulation of voltage-gated Ca^{2+} entry and Ca^{2+} release from intracellular stores [16,23,24]. However, the above mentioned increases in $[Ca^{2+}]_{mit}$ were transient and restricted to a pool of mitochondria close to sites of Ca^{2+} entry or release [23,24]. The recent introduction of low-affinity, targeted chameleons [38] has confirmed that $[Ca^{2+}]_{mit}$ may reach values above 200 μM, the sensitivity limit of these probes, stressing that $[Ca^{2+}]_{mit}$ levels actually rise substantially and the requirement of low-affinity probes for actual measurements of $[Ca^{2+}]_{mit}$, particularly when a mitochondrial Ca^{2+} overload is to be measured. Using the low-affinity, mitochondria-targeted aequorin, we find that $A\beta_{25–35}$ and $A\beta_{1–42}$ oligomers, but not fibrils, induce a massive mitochondrial Ca^{2+} overload that reaches values close to the mM level. As aequorin is consumed by the high Ca^{2+} level achieved, the results suggest that, at variance with stimulation with high K^+, most mitochondria take up Ca^{2+} when cells are stimulated by $A\beta_{1–42}$ oligomers. As mitochondrial Ca^{2+} uptake through the mitochondrial Ca^{2+} uniporter requires high $[Ca^{2+}]_{cyt}$ levels, these results suggest that $A\beta_{1–42}$ oligomers promote a massive entry of Ca^{2+}, large and sustained enough to activate the mitochondrial Ca^{2+} uniporter of most mitochondria.

It has been reported that mitochondrial Ca^{2+} overload may promote mPTP opening and apoptotic cell death [26,39]. Our results indicate that mitochondrial Ca^{2+} overload contributes to the apoptotic cell death induced by Aβ oligomers. This view is supported by the findings that $A\beta_{1–42}$ oligomers promote i)a mitochondrial Ca^{2+} overload in the whole mitochondrial population, ii)mitochondrial calcein quenching in a cyclosporin sensitive manner, iii)release of cytochrome c, iv)apoptosis as determined by TUNEL assay and v)cell death, again in a cyclosporin A-sensitive manner. Furthermore, inhibition of mitochondrial Ca^{2+} uptake by low concentrations of FCCP inhibit both cytochrome c release and cell death without preventing $A\beta_{1–42}$ oligomers-induced increases in $[Ca^{2+}]_{cyt}$ or decreasing cell ATP levels. Finally, $A\beta_{1–42}$ oligomers induce ROS production and this effect is prevented by low concentrations of FCCP. Taken together, our results suggest that the large and sustained entry of Ca^{2+} induced by $A\beta_{1–42}$ oligomers, an effect mimicked by larger concentrations of the toxic fragment $A\beta_{25–35}$, activate the mitochondrial Ca^{2+} uniporter of most mitochondria leading to a mitochondrial Ca^{2+} overload. This effect may promote mPTP opening by itself or, cooperate with the excess of ROS production promoted by the own mitochondrial Ca^{2+} overload. Finally, mPTP opening allows release of pro-apoptotic factors including cytochrome c leading to apoptosis and cell death (see proposed model in Fig. 9). This view resembles the mechanism of excitotoxicity reported for glutamate. In fact, glutamate-induced neuron death requires mitochondrial Ca^{2+} uptake [40]. In addition, low concentrations of FCCP have been reported to prevent mitochondrial Ca^{2+} uptake and cell death induced by NMDA [41]. Finally, glutamate induces also ROS production and this effect is prevented by mitochondrial uncoupling and blockers of the mitochondrial Ca^{2+} uniporter [32]. Whereas this mechanism may contribute largely to cell death induced by Aβ oligomers, our results do not exclude that additional mechanisms might contribute to this toxicity. For example, it has been reported that intracellular Aβ species may also interact with mitochondria in AD mouse models and affected AD brains [7–9] and this interaction may promote apoptosis and cell death. It remains to be established whether mitochondrial alterations induced by mitochondria-bound Aβ species cooperate with mitochondrial Ca^{2+} overload to promote cell death.

The above findings indicate that mitochondrial Ca^{2+} overload contributes to the neurotoxicity induced by $A\beta_{1–42}$ oligomers. Accordingly, any strategy intended to prevent specifically mitochondrial Ca^{2+} uptake could potentially protect neurons against $A\beta_{1–42}$ oligomers toxicity. Among the most promising agents for neuroprotection against AD are a series of classic NSAIDs [5,42,43]. Recent evidence indicates that neuroprotection afforded by NSAIDs is due to a mechanism other than their anti-inflammatory activity. This view is based in that some, but not all NSAIDs show neuroprotection and that structural analogs of classic NSAIDs lacking anti-inflammatory activity like, for instance, R-flurbiprofen, offer protection as well [43]. Some NSAIDs including R-flurbiprofen have been reported to target and inhibit γ-secretase activity at rather large concentrations (100 μM) leading to a lower Aβ burden [44,45]. We show here

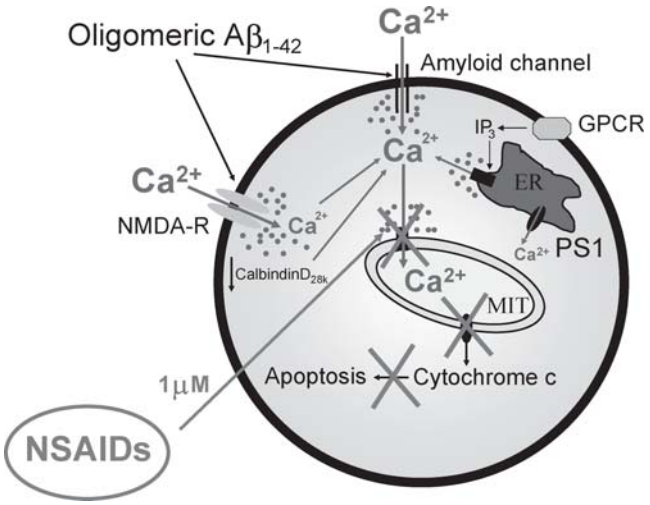

Figure 9. A model of Aβ-induced toxicity and neuroprotection by NSAIDs based on mitochondrial Ca^{2+}. $A\beta_{1-42}$ oligomers and the toxic fragment $A\beta_{25-35}$ induce a large entry of Ca^{2+} through the plasma membrane likely mediated by formation of amyloid channels and/or NMDA receptors. This entry promotes in a sequential manner mitochondrial Ca^{2+} overload, ROS production, mPTP opening, cytochrome c release, apoptosis and cell death. Other factors related to AD may favor mitochondrial Ca^{2+} overload including exaggerated IP_3-induced release of Ca^{2+} from the ER in loss of function PS1 mutants related to familial AD and/or decreased abundance of endogenous Ca^{2+} buffers as calbindinD28k during aging or sporadic AD. NSAIDs, at low concentrations (1 μM), depolarize partially mitochondria and inhibit mitochondrial Ca^{2+} overload, thus preventing cytochrome c release and apoptosis induced by Aβ oligomers.
doi:10.1371/journal.pone.0002718.g009

that, at very low concentrations (1 μM), NSAIDs depolarize mitochondria to the same extent than low concentrations of FCCP, inhibit mitochondrial Ca^{2+} overload induced by Aβ oligomers without preventing Ca^{2+} entry through the plasma membrane, prevent ROS production induced by $A\beta_{1-42}$ oligomers and inhibit Aβ oligomers-induced cytochrome c release and cell death. Accordingly we propose a novel mechanism of neuroprotection against soluble $A\beta_{1-42}$ species by non-specific NSAIDs based on the primary inhibition of mitochondrial Ca^{2+} overload and prevention of the ensuing mPTP opening an downstream steps to cell death (Fig. 9). Notice that, at these low concentrations, NSAIDs have little or no effect on γ-secretase activity whereas fitting the concentration range achieved in brains by human therapeutic dose [45]. We must stress that these results have been obtained mainly in cerebellar granule cells, a brain area generally considered not affected earlier in AD. However, as mentioned above, neuropathological studies have shown frequent and varied cerebellar changes in the late stages of the disease [1]. Nevertheless, we show that $A\beta_{1-42}$ oligomers also induced large increases in $[Ca^{2+}]_{cyt}$ and $[Ca^{2+}]_{mit}$ in cortical neurons as well as rises in $[Ca^{2+}]_{cyt}$ in hippocampal neurons.

The mechanism of inhibition of mitochondrial Ca^{2+} uptake by NSAIDs is most likely mediated by mitochondrial depolarization. This view is supported by i)the chemical structure of NSAIDs resembling mitochondrial uncouplers, ii)the release of Ca^{2+} induced by salicylate in Ca^{2+}-overloaded cells and iii)direct TMRM fluorescence measurements showing NSAID-induced mitochondrial depolarization. In addition, uncoupling activity is considered a common characteristic of anti-inflammatory agents with an ionizable group [46]. It may seem surprising that a small mitochondrial depolarization be enough to inhibit largely mitochondrial Ca^{2+} uptake. However, several facts support this view. First the Ca^{2+} channel associated to the mitochondrial Ca^{2+} uniporter is inwardly rectifying, making it especially effective for Ca^{2+} uptake into energized mitochondria [47]. In this scenario, a mild mitochondrial depolarization will decrease largely the Ca^{2+} current through the mitochondrial Ca^{2+} uniporter. Second, the Nernst's equilibrium for Ca^{2+} across mitochondria predicts that a 50% fall in $\Delta\Psi$ reduces the free mitochondrial $[Ca^{2+}]$ that can be reached at equilibrium by 1,000 fold [23]. This prediction is based on the huge $\Delta\Psi$ built in respiring mitochondria and the fact that Ca^{2+} is a divalent cation present at extremely low concentrations (100 nM) in resting mitochondria. Thus, it is thermodynamically possible that even small drops in $\Delta\Psi$ could influence dramatically the $[Ca^{2+}]_{mit}$ increase achieved during cell stimulation. In support of this view, we have shown recently that small drops in $\Delta\Psi$ of a few tens of mVs are enough to prevent largely mitochondrial Ca^{2+} uptake [30].

Interestingly, other AD-related factors seemingly independent of Aβ species may contribute as well to mitochondrial Ca^{2+} overload and, perhaps, to neurotoxicity. For example, in familial AD, loss of function presenilin 1 mutants show exaggerated Ca^{2+} release from intracellular stores due to either defective Ca^{2+} leak from the ER or increased activity of Ca^{2+} release channels at ER [48–50, but see also 51 for alternative results]. The close coupling between ER and mitochondria [52] may favor mitochondrial Ca^{2+} overload in patients carrying these mutations. Further research is required to support this view. If that were the case, the possible PS1 mutation-mediated mitochondrial Ca^{2+} overload and ensuing neuron damage should be limited by NSAIDs. An even more important factor, at least from the point of view of the potential number of patients affected, could be the reported depletion of endogenous Ca^{2+} buffers, particularly calbindinD28k, in selected brain regions during aging and sporadic AD [53,54]. A diminished cytosolic Ca^{2+} buffer capacity may place mitochondria at risk of Ca^{2+} overload during normal neural activity, a process that should be ameliorated by NSAIDs. Therefore, our results point to a pivotal role of mitochondrial Ca^{2+} overload in $A\beta_{1-42}$ oligomers toxicity and AD. Interestingly, the mitochondrial Ca^{2+} overloads likely induced by AD related processes such as Aβ oligomers (shown here), excitotoxicity [40], excess Ca^{2+} release from ER [49] and loss of endogenous Ca^{2+} buffers [53,54] could be all ameliorated by low NSAID concentrations, regardless of the source of Ca^{2+} excess being either intracellular or extracellular.

Materials and Methods

Materials

Wistar rats were obtained from the Valladolid University animal facility. Fura2/AM, TMRM, DAPI, CM-H2DCFDA, n coelenterazine, the cytochrome c antibody, Alexa 488 α mouse IgG and Alexa F594 α rabbit IgG were purchased from Invitrogen (Barcelona, Spain). DMEM (ref. 41966-029), fetal bovine serum, horse serum, neurobasal medium, B27, penicillin and streptomycin are from Gibco (Barcelona, Spain). Papain solution is from Worthington (Lakewood, NJ). The kit for TUNEL assay is from Roche Diagnostics (Penzberg, Germany). Aβ peptides were purchased from Bachem AG (Bubendorf, Switzerland). The mouse anti β-tubulin III is from Covance (Princeton, USA) and the rabbit anti-GFAP is from Sigma (Madrid, Spain). The mGA plasmid was kindly donated by P. Brulet (Gif-sur-Yvette, France). Hypothalamic GT1 neural cells were provided by R. Weiner (San Francisco, USA). Other reagents and chemicals were obtained either from Sigma or Merck.

Cell Cultures

Cerebellar granule cells were obtained from 5-day old Wistar rat pups killed by dislocation followed by decapitation as reported previously [55]. Cortical neurons were obtained from P0 Wistar rat pups following the protocol reported by Murphy *et al.* [56]. Hippocampal neurons were prepared from P0 Wistar rat pups as reported by Brewer *et al.* [57] with the modifications introduced by Perez-Otano *et al.* [58]. Briefly, after brain removal, meninges were discarded and the hippocampus was separated from cortex. Hippocampal tissue was cut in small pieces, transferred to papain solution and incubated at 37° C for 30 minutes with occasional gentle shaking. Tissue pieces were washed with neurobasal medium and dissociated into a single cell suspension. Hippocampal cells were plated onto collagen-coated, 12 mm diameter glass coverslips at 40×10^3 cells/dish, and grown in Neurobasal Medium supplemented with B27 and 10% horse serum. Cells were cultured for 7–10 days before experiments. Cerebellar granule cells and cortical neurons were plated on poly-L-lysine coated, 12 mm diameter glass coverslips and cultured in high-glucose, low K^+, Dulbeccos modified Eagles medium (DMEM, ref. 41966-029. Gibco, Spain) plus 10% fetal bovine serum, 5% horse serum, 100 u ml^{-1} penicillin and 100 μg ml^{-1} streptomycin for 2 days. Then the culture medium was replaced by Satos medium [59] plus 5% horse serum to avoid excessive proliferation of glia and cultured for 2–4 (cerebellar) or 3–5 (cortical) days before experiments. GT1 neural cells were grown in DMEM with 10% fetal bovine serum, 5% horse serum, 100 u ml^{-1} penicillin and 100 μg ml^{-1} streptomycin.

Preparation of Aβ oligomers and fibrils

$A\beta_{1-42}$ oligomers and fibrils were prepared as reported previously by Klein and Dahlgren et al. [17,20]. Briefly, $A\beta_{1-42}$ was initially dissolved to 1 mM in hexafluoroisopropanol and separated into aliquots in sterile microcentrifuge tubes. Hexafluoroisopropanol was removed under vacuum in a speed vac., and the peptide film was stored desiccated at −20°C. For the aggregation protocol, the peptide was first resuspended in dry dimethyl sulfoxide to a concentration of 5 mM and treated differently for preparation of oligomers and fibrils. For preparation of oligomers, Hams F-12 was added to bring the peptide to a final concentration of 100 μM and incubated at 4°C for 24 h. The preparation was then centrifuged at 14,000×g for 10 min at 4°C to remove insoluble aggregates (protofibrils and fibrils) and the supernatants containing soluble $A\beta_{1-42}$ oligomers were transferred to clean tubes and stored at 4°C. For preparation of fibrils, the peptide resuspended in dimethyl sulfoxide at 5 mM concentration was diluted in 10 mM HCl to bring the peptide to a final concentration of 100 μM and incubated at 37°C for 24 h. Actual concentrations of both oligomers and fibrils were measured by amino acid analysis. $A\beta_{25-35}$ was solved in PBS at a concentration of 1 mM, sonicated 3 times and stored at −20°C. For experiments, $A\beta_{25-35}$ was solved in medium at a final concentration of 20 μM.

Amino Acid analysis

Samples of both $A\beta_{1-42}$ oligomers and fibrils in glass tubes were extensively vacuum dried in a speed-vac. Hydrolysis was performed using a 5.9 HCl solution containing 0.1% phenol. Norleucine was added to the hydrolytic solution as an internal standard. The tubes were sealed under vacuum and the hydrolysis was performed during 24 h at 110°C. Subsequently, the samples were vacuum dried. Finally, the samples were injected into a Biochrom 30 amino acid analyzer. Both composition and concentration data was obtained from the chromatogram.

PAGE-SDS and silver staining

A standard 17% PAGE-SDS was prepared and 10 μl samples of either $A\beta_{1-42}$ oligomers or fibrils at a 40 μM concentration were incubated with 1X loading buffer. The samples were loaded in the gel without boiling and the gel was run at constant amperage of 20 mA. The gels were subsequently fixed with a freshly prepared solution of 50% methanol, 12% acetic acid, 0.02% paraformaldehyde for at least 1h. Then, the gel was washed three times with 50% ethanol. The next step consisted on an incubation of the gel for 1 min in 0.2 mg/ml NaS_2O_3. Subsequently, the gel was washed three times with miliQ water for 20 seconds. Then, the gel was incubated for 20 minutes in 2 mg/ml $AgNO_3$ in 0.025% formaldehyde. After two 20-second washes with miliQ water, color was allowed to develop using a solution consisting of 60 mg/ml Na_2CO_3, 0.02% formaldehyde, 0.004 mg/ml NaS_2O_3. After the bands appear, the gel was washed twice with miliQ water and the reaction was stopped using a 50% methanol, 12% acetic acid solution.

Electron microscopy

A 10 μl sample of $A\beta_{1-42}$ fibrils (40 μM) was applied to a 200 mesh Formvar-coated copper grid and incubated for 15 minutes at room temperature. The sample was then wicked off with filter paper, washed briefly by placing the grid face down on a droplet of water, and stained by transferring the grid face down on a droplet of 2% uranyl acetate for 2 minutes before wicking off the solution and air drying. Grids were visualized in a JEOL transmission electron microscope.

Fluorescence imaging of $[Ca^{2+}]_{cyt}$ and in situ immunofluorescence

Coverslips containing cells were incubated in standard medium containing (in mM) NaCl 145, KCl 5, $CaCl_2$ 1, $MgCl_2$ 1, glucose 10 and Hepes 10 (pH, 7.42) and loaded with 4 μM fura2/AM or fura4F/AM for 60 min at room temperature. Then coverslips were placed on the heated stage of an inverted microscope (Nikon Diaphot), perfused continuously with the same prewarmed standard medium containing and epi-illuminated alternately at 340 and 380 nm. Light emitted above 520 nm was recorded with a Magical Image Processor (Applied Imaging). Pixel by pixel ratios of consecutive frames were captured and $[Ca^{2+}]_{cyt}$ was estimated from these ratios as previously reported [16]. For differential identification of neurons and glia, the single cell content of β-tubulin III and glial fibrillary acidic protein (GFAP) were assessed by indirect inmunofluorescence in the same cells used for calcium imaging as reported previously [55]. Briefly, after calcium imaging, cells were fixed with p-formaldehyde and incubated with anti β tubulin III (1:400) and anti GFAP (1:200) for 1 h at 37°C. Then, cells were washed and incubated with 1:100 labeled anti IgG antibodies. Nuclei were stained by incubation with DAPI 0,2 μg/ml for 5 min.

Bioluminescence imaging of $[Ca^{2+}]_{mit}$

Cells were transfected with the mGA plasmid using a Nucleofector II® device and the VPG-1003 transfection kit (Amaxa Biosystems, Cologne, Germany). The mGA probe contain a mutated, low affinity aequorin targeted to mitochondria and a GFP sequence to help select transfected neurons [25]. After 24 h, cells were incubated for 1 h with 1 μM n coelenterazine, washed and placed into a perfusion chamber thermostated to 37 °C under a Zeiss Axiovert S100 TV microscope and perfused at 5–10 ml/min with test solutions based on the standard perfusing solution described above prewarmed at 37°C. At the end of each

experiment, cells were permeabilized with 0.1 mM digitonin in 10 mM $CaCl_2$ to release all the residual aequorin counts. Bioluminescence images were taken with a Hamamatsu VIM photon counting camera handled with an Argus-20 image processor. Photonic emissions were integrated for 10 s periods. Photons/cell in each image were quantified using the Hamamatsu Aquacosmos software. Total counts per cell ranged between $2{\cdot}10^3$ and $2{\cdot}10^5$ and noise was (mean±SD) 1±1 counts per second (c.p.s.) per typical cell area (2000 pixels). Data were first quantified as rates of photoluminescence emission/total c.p.s remaining at each time (% of remaining counts) and divided by the integration period (L/L_{TOTAL} in s^{-1}). Emission values of less than 4 c.p.s were not used for calculations. Calibrations in terms of $[Ca^{2+}]_{mit}$ were performed using as reported previously [23]. In some experiments, cells were permeabilized with digitonin 20 μM in "intracellular" medium of the following composition 130 mM KCl, 10 mM NaCl, 1 mM $MgCl_2$, 1 mM K_3PO_4, 0,2 mM EGTA, 1 mM ATP, 20 μM ADP, 2 mM succinate, 20 mM HEPES/KOH, pH, 6.8. Then, the cells were incubated with the same medium containing 200 nM Ca^{2+} (buffered with EGTA) with or without NSAIDs for 5 min. Then, perfusion was switched to "intracellular" medium containing 5 μM Ca^{2+} (with or without NSAID). Further details have been reported previously [16,23,25].

Mitochondrial permeability transition pore (mPTP)

mPTP opening was assessed directly by the calcein/cobalt method [28]. Cells were co-loaded with calcein-AM 1 μM and $CoCl_2$ 1 mM for 30 min at 37°C and subjected to conventional fluorescence imaging or confocal microcopy. Fluorescence traces from individual cells were normalized relative to the value before addition of test solutions and averaged. Background fluorescence corresponding to regions of interest devoid of cells was subtracted. In some experiments, cells were incubated with cyclosporin A 1 μM for 15 min before recordings.

ROS Formation

ROS formation was evaluated in live neurons using CM-H2DCFDA as reported by De Felice *et al.* [37]. Cerebellar granule cell cultures were incubated for 4 h at 37°C with vehicle or 500 nM $Aβ_{1–42}$ in the absence or in the presence of FCCP 100 nM and R-flurbiprofen 1 μM. ROS formation was assessed using 2 μM CM-H2DCFDA with 40 min of probe loading. Then neurons were superfused for 5 min with prewarmed (37°C) PBS. Fluorescence in cells was immediately visualized using the Zeiss S100 TV inverted microscope, a FITC filter set, an OrcaER digital camera from Hamamatsu and the Hamamatsu Aquacosmos software.

Mitochondrial potential (ΔΨ)

The effects of treatments on ΔΨ were estimated by fluorescence imaging in cells loaded with the ΔΨ sensitive probe TMRM as reported previously [29–31]. Briefly, cells were loaded with TMRM (10 nM) for 30 min at room temperature, placed on the perfusion chamber of a Zeiss Axiovert S100 TV inverted microscope and superfused continuously with the prewarmed (37°C) standard medium described above. Fluorescence images were taken at 10 s intervals with a Hamamatsu VIM photon counting camera handled with an Argus-20 image processor. Traces from individual cells were normalized relative to the value before the addition of either vehicle or treatment and averaged. Background fluorescence -after collapse of the mitochondrial potential induced by 10 μM FCCP- was subtracted. Location of TMRM staining and fluorescence intensity ratios of TMRM in mitochondrial and cytosolic areas was tested by confocal microcopy in cells stained with both TMRM and mitotracker green.

Cytochrome c release

Cytochrome c release from mitochondria was tested by immunofluorescence and conventional or confocal microscopy. Cells were treated under the various experimental conditions for 72 h and fixed. Location of cytochrome c was tested by indirect immunofluorescence. In conventional fluorescence, nuclei were identified by DAPI staining. Confocal images were obtained using a BIO-RAD laser scanning system (Radiance 2100) coupled to a Nikon eclipse TE2100U, inverted microscope. For quantification of cytochrome c release by confocal microscopy, the relative abundance (%) of cells showing diffuse vs. punctate immunofluorescence was calculated [60].

Cell death and apoptosis

Cells were plated in wells at about $5{\times}10^4$ cells/ml and treated with test solutions for 72 h. Cell death was estimated in the same samples by staining with fluorescein diacetate (FDA, 50 μg/ml, 3 min) and propidium iodide (PI, 20 μg/ml, 30 s) and assessed by fluorescence microscopy using a Nikon Eclipse 80i microscope coupled to a DM 1200C digital camera using a 20x objective. For determination of apoptotic cells at the single cell level, cells were plated at about $5{\times}10^4$ cells/ml and incubated with test solutions for 72 h. Apoptotic cells were revealed by the terminal deoxynucleotidyl transferase-mediated dUTP nick-end labeling (TUNEL) method by fluorescence imaging and a cell death detection kit following the protocol provided by the manufacturer.

Cell ATP levels

Cerebellar granule cells were plated in 4-well plates and cultured with test solutions for 72 h. Then, cells were washed twice with PBS at 37°C and 1 ml of boiling 20 mM Tris, pH, 7.75 and 4 mM EDTA was added. After 2 min, samples were centrifuged for 4 min at 10.000 g. ATP was measured later from the supernatant by the luciferin-luciferase assay using a Cairn photon counting device (Cairn Research, UK) and a standard curve prepared using pure ATP over a 10^{-5} to 10^{-9} M concentration range.

Statistics

When only two means were compared, Student's t test was used. For more than two groups, statistical significance of the data was assessed by ANOVA and compared using Bonferroni's multiple comparison test. Differences were considered significant at $p<0,05$.

Supporting Information

Figure S1 Characterization of Aβ oligomers and fibrils. *A.* SDS-PAGE and silver staining of an oligomeric $Aβ_{1–42}$ sample. Arrows point to bands reflecting the presence of monomers, dimers and tetramers. Representative of 3 experiments. *B*, SDS-PAGE and silver staining of a fibrillar $Aβ_{1–42}$ sample. Arrows point to bands reflecting the presence of monomers, dimers, tetramers. Some larger oligomerization species also are apparent in the gel. In addition, a certain amount of large molecular weight fibrils incapable of entering the separating gel is also pointed on top. Representative of 3 experiments. *C.* Electron microscopy was used in order to characterize $Aβ_{1–42}$ fibrils. Negative staining using uranyl acetate undoubtedly showed the presence of large fibrils in solution. Most fibrils were similar in width and with a length that

usually varied between 200 and 800 nm. Bar represents 200 nm. Representative of 6 experiments. $A\beta_{1-42}$ oligomers and fibrils were also characterized by amino acid analysis for testing actual concentration values and composition (data not shown).
Found at: doi:10.1371/journal.pone.0002718.s001 (9.36 MB TIF)

Figure S2 $A\beta_{25-35}$ induces apoptosis and cell death in cerebellar granule cells. *A.* Cerebellar granule cells were cultured for 72 h in vehicle (control) or $A\beta_{25-35}$ (20 μM) and apoptosis was tested by TUNEL assay. Pictures show nuclei (blue) and apoptotic cells (purple). Bars show % of apoptotic cells (n = 3; *$p<0,05$). Scale bar represents 10 μm. *B.* Cerebellar granule cells were cultured for 72 h with vehicle (control) or $A\beta_{25-35}$ (20 μM) and cell death was assessed by staining with FDA (green, living cells) and PI (red, dead cells). Bars show % of dead cells (n = 3; *$p<0$ 05 *vs.* control). Scale bar represents 10 μm.
Found at: doi:10.1371/journal.pone.0002718.s002 (6.71 MB TIF)

Figure S3 FCCP prevents the mitochondrial (but not the cytosolic) Ca^{2+} rise and cytochrome c release induced by $A\beta_{25-35}$. *A.* Cerebellar granule cells expressing mGA were subjected to bioluminescence for $[Ca^{2+}]_{mit}$ measurements. FCCP 100 nM inhibits the increase in $[Ca^{2+}]_{mit}$ induced by $A\beta_{25-35}$ (20 μM, 17 cells, 3 experiments). After washout of FCCP, $A\beta_{25-35}$ was able to increase $[Ca^{2+}]_{mit}$. *B.* Cerebellar granule cells were loaded with fura2/AM and subjected to fluorescence imaging for $[Ca^{2+}]_{cyt}$ measurements. FCCP 100 nM failed to inhibit the increase in $[Ca^{2+}]_{cyt}$ induced by $A\beta_{25-35}$ (20 μM) (n = 273 cells, 3 experiments). *C.* Immunofluorescence against cytochrome c was assessed by confocal microscopy in cerebellar granule cells treated with vehicle (Control), $A\beta_{25-35}$ 20 μM (Aβ) and 20 μM $A\beta_{25-35}$ + FCCP 100 nM (Aβ+FCCP) for 72 h. $A\beta_{25-35}$ promotes diffusion of cytochrome c that normally shows a punctate staining reflecting mitochondrial location. 100 nM FCCP prevented diffusion of cytochrome C. Scale bar represents 10 μm. *D.* Bars show % of cells showing diffuse staining for cytochrome c (reflecting cytochrome c release). $A\beta_{25-35}$ (20 μM) increases the percent of cells showing diffuse staining an this effect was inhibited by FCCP 100 nM. $^{a}p<0,05$ vs. control; $^{b}p<0,05$ vs. Aβ treated cells. Bars are mean±SEM of 3 independent experiments.
Found at: doi:10.1371/journal.pone.0002718.s003 (2.27 MB TIF)

Figure S4 Aβ oligomers induce ROS formation that is prevented by FCCP and R-flurbiprofen. Cerebellar granule cells were incubated for 4 h with vehicle, $A\beta_{1-42}$ oligomers (500 nM) and oligomers plus FCCP 100 nM or R-flurbiprofen. Then, ROS production was imaged using the ROS-sensitive probe CM-H2DCFDA. $A\beta_{1-42}$ oligomers induced an increase in fluorescence compared to the vehicle that was prevented by FCCP and R-flurbiprofen. The Pictures are representative of 5–9 microscopic fields in at least 3 independent experiments for each condition. Addition of FCCP or R-flurbiprofen alone produced similar results than vehicle (data not shown).
Found at: doi:10.1371/journal.pone.0002718.s004 (2.83 MB TIF)

Figure S5 NSAIDs prevent cytochrome c release and cell death induced by $A\beta_{25-35}$. *A.* Cerebellar granule cells were treated with $A\beta_{25-35}$ (20 μM) for 72 h with or without 1 μM R-flurbiprofen or 100 μM salicylate and fixed for analysis of cytochrome c location using confocal microscopy. Control cells showed a punctate distribution of cytochrome c. Scale bar represents 10 μm. $A\beta_{25-35}$ treated cells show a more diffuse pattern of cytochrome c whereas cells treated with $A\beta_{25-35}$ and R-flurbiprofen show a punctate pattern similar to control cells. Bars show the relative abundance (%) of cells showing diffuse immunostaining in control cells, cells treated with $A\beta_{25-35}$ and cells treated with $A\beta_{25-35}$ plus 1 μM R-flurbiprofen (B) or 100 μM salicylate (C). (*$p<0,05$ vs. control; #$p<0,05$ vs. Aβ). *D.* Effects of ibuprofen (Ibu), indomethacin (Indo) and sulindac sulfide (Sul), all tested at 1 μM, on cell death induced by $A\beta_{25-35}$ (20 μM) as assessed by dye exclusion studies. *E.* Effects of R- and S-flurbiprofen (Rf and Sf), both tested at 1 μM, on cell death induced by $A\beta_{25-35}$. *$p<0,05$ vs. control; $^{\#}p<0,05$ vs. Aβ. All data are representative of 3 experiments.
Found at: doi:10.1371/journal.pone.0002718.s005 (2.10 MB TIF)

Acknowledgments

We thank Ms. Carmen Román for technical assistance, Mr. Alberto Sánchez-Guijo for help with confocal microscopy, Prof. Philip Brulet for the gift of mGA plasmid, Prof. Richard Weiner for the GT1 neural cell line and Prof. Isabel Perez-Otaño for help with hippocampal cell culture.

Author Contributions

Conceived and designed the experiments: SSB IRC CV LN. Performed the experiments: SSB RAV IRC LN. Analyzed the data: SSB CV LN. Wrote the paper: CV LN.

References

1. Wegiel J, Wisniewski HM, Dziewiatkowski J, Badmajew E, Tarnawski M, et al. (1999) Cerebellar atrophy in Alzheimer's disease-clinicopathological correlations. Brain Res 818: 41–50.
2. Allen JW, Eldadah BA, Faden AI (1999) Beta-amyloid-induced apoptosis of cerebellar granule cells and cortical neurons: exacerbation by selective inhibition of group I metabotropic glutamate receptors. Neuropharmacology 38: 1243–1252.
3. Canu N, Calissano P (2003) In vitro cultured neurons for molecular studies correlating apoptosis with events related to Alzheimer disease. Cerebellum 2: 270–278.
4. Plant LD, Webster NJ, Boyle JP, Ramsden M, Freir DB, et al. (2006) Amyloid beta peptide as a physiological modulator of neuronal 'A'-type K^+ current. Neurobiol Aging 11: 1673–1683.
5. McGeer PL, Rogers J, McGeer EG (2006) Inflammation, anti-inflammatory agents and Alzheimer disease: the last 12 years. J Alzheimers Dis 9: 271–276.
6. Canevari L, Abramov AY, Duchen MR (2004) Toxicity of amyloid beta peptide: tales of calcium mitochondria and oxidative stress. Neurochem Res 29: 637–650.
7. Caspersen C, Wang N, Yao J, Sosunov A, Chen X, et al. (2005) Mitochondrial Abeta: a potential focal point for neuronal metabolic dysfunction in Alzheimer's disease. FASEB J 19: 2040–2041.
8. Manczak M, Anekonda TS, Henson E, Park BS, Quinn J, et al. (2006) Mitochondria are a direct site of A beta accumulation in Alzheimer's disease neurons: implications for free radical generation and oxidative damage in disease progression. Hum Mol Genet 15: 1437–1449.
9. Reddy PH, Beal MF (2008) Amyloid beta, mitochondrial dysfunction and synaptic damage: implications for cognitive decline in aging and Alzheimer's disease. Trends Mol Med 14: 45–53.
10. LaFerla FM (2002) Calcium dyshomeostasis and intracellular signalling in Alzheimer's Disease. Nat Rev Neurosci 3: 862–872.
11. Abramov AY, Canevari L, Duchen MR (2003) Changes in intracellular calcium and glutathione in astrocytes as the primary mechanism of amyloid neurotoxicity. J Neurosci 23: 5088–5095.
12. Marx J (2007) Alzheimer's disease: Fresh evidence points to an old suspect: calcium. Science 318: 384–385.
13. Klein WL, Stine WB Jr, Teplow DB (2004) Small assemblies of unmodified amyloid beta-protein are the proximate neurotoxin in Alzheimer's disease. Neurobiol Aging 25: 569–580.
14. Haass C, Selkoe DJ (2007) Soluble protein oligomers in neurodegeneration: lessons from the Alzheimer's amyloid beta-peptide. Nat Rev Mol Cell Biol 8: 101–112.
15. Guo Q, Christakos S, Robinson N, Mattson MP (1998) Calbindin D28k blocks the proapoptotic actions of mutant presenilin 1: reduced oxidative stress and preserved mitochondrial function. Proc Natl Acad Sci USA 95: 3227–3232.
16. Núñez L, Senovilla L, Sanz-Blasco S, Chamero P, Alonso MT, et al. (2007) Bioluminescence imaging of mitochondrial Ca^{2+} dynamics in soma and neurites of individual adult mouse sympathetic neurons. J Physiol 580: 385–395.
17. Klein WL (2002) Abeta toxicity in Alzheimer's disease: globular oligomers (ADDLs) as new vaccine and drug targets. Neurochem Int 41: 345–352.

18. Burdick D, Soreghan B, Kwon M, Kosmoski J, Knauer M, et al. (1992) Assembly and aggregation properties of synthetic Alzheimer's A4/beta amyloid peptide analogs. J Biol Chem 267: 546–554.
19. Kawahara M, Kuroda Y (2001) Intracellular calcium changes in neuronal cells induced by Alzheimer's beta-amyloid protein are blocked by estradiol and cholesterol. Cell Mol Neurobiol 21: 1–13.
20. Dahlgren KN, Manelli AM, Stine WB Jr, Baker LK, Krafft GA, et al. (2002) Oligomeric and fibrillar species of amyloid-beta peptides differentially affect neuronal viability. J Biol Chem 277: 32046–32053.
21. Deshpande A, Mina E, Glabe C, Busciglio J (2006) Different conformations of amyloid beta induce neurotoxicity by distinct mechanisms in human cortical neurons. J Neurosci 26: 6011–6018.
22. Villalobos C, Núñez L, Chamero P, Alonso MT, García-Sancho J (2001) Mitochondrial $[Ca^{2+}]$ oscillations driven by local high $[Ca^{2+}]$ domains generated by spontaneous electric activity. J Biol Chem 276: 40293–40297.
23. Villalobos C, Núñez L, Montero M, García AG, Alonso MT, et al. (2002) Redistribution of Ca^{2+} among cytosol and organella during stimulation of bovine chromaffin cells. FASEB J 16: 343–353.
24. Montero M, Alonso MT, Carnicero E, Cuchillo-Ibáñez I, Albillos A, et al. (2000) Chromaffin-cell stimulation triggers fast millimolar mitochondrial Ca^{2+} transients that modulate secretion. Nat Cell Biol 2: 57–61.
25. Rogers KL, Stinnakre J, Agulhon C, Jublot D, Shorte SL, et al. (2005) Visualization of local Ca^{2+} dynamics with genetically encoded bioluminescent reporters. Eur J Neurosci 21: 597–610.
26. Kruman II, Mattson MP (1999) Pivotal role of mitochondrial calcium uptake in neural cell apoptosis and necrosis. J Neurochem 72: 529–540.
27. Norenberg MD, Rao KV (2007) The mitochondrial permeability transition in neurologic disease. Neurochem Int 50: 983–997.
28. Petronilli V, Miotto G, Canton M, Colonna R, Bernardi P, et al. (1998) Imaging the mitochondrial permeability transition pore in intact cells. Biofactors 8: 263–272.
29. Núñez L, Valero RA, Senovilla L, Sanz-Blasco S, García-Sancho J, et al. (2006) Cell proliferation depends on mitochondrial Ca^{2+} uptake: inhibition by salicylate. J Physiol 571: 57–73.
30. Valero RA, Senovilla L, Núñez L, Villalobos C (2008) The role of mitochondrial potential in control of calcium signals involved in cell proliferation. Cell Calcium. In press.
31. Voronina SG, Barrow SL, Gerasimenko OV, Petersen OH, Tepikin AV (2004) Effects of secretagogues and bile acids on mitochondrial membrane potential of pancreatic acinar cells: comparison of different modes of evaluating DeltaPsim. J Biol Chem 279: 27327–27338.
32. Duan Y, Gross RA, Sheu SS (2007) Ca^{2+}-dependent generation of mitochondrial reactive oxygen species serves as a signal for poly(ADP-ribose) polymerase-1 activation during glutamate excitotoxicity. J Physiol 585: 741–758.
33. Brocard JB, Tassetto M, Reynolds IJ (2001) Quantitative evaluation of mitochondrial calcium content in rat cortical neurones following a glutamate stimulus. J Physiol 531: 793–805.
34. Demuro A, Mina E, Kayed R, Milton SC, Parker I, et al. (2005) Calcium dysregulation and membrane disruption as a ubiquitous neurotoxic mechanism of soluble amyloid oligomers. J Biol Chem 280: 17294–17300.
35. Simakova O, Arispe N (2006) Early and late cytotoxic effects of external application of the Alzheimer's Abeta result from the initial formation and function of Abeta ion channels. Biochemistry 45: 5907–5915.
36. Arispe N, Diaz JC, Simakova O (2007) Abeta ion channels: Prospects for treating Alzheimer's disease with Abeta channel blockers. Biochim Biophys Acta 1768: 1952–1965.
37. De Felice FG, Velasco PT, Lambert MP, Viola K, Fernandez SJ, et al. (2007) Abeta oligomers induce neuronal oxidative stress through an N-methyl-D-aspartate receptor-dependent mechanism that is blocked by the Alzheimer drug memantine. J Biol Chem 282: 11590–11601.
38. Palmer AE, Giacomello M, Kortemm T, Hires SA, Lev-Ram V, et al. (2006) Ca^{2+} indicators based on computationally redesigned calmodulin-peptide pairs. Chem Biol 13: 521–530.
39. Dubinsky JM, Levi Y (1998) Calcium-induced activation of the mitochondrial permeability transition in hippocampal neurons. J Neurosci Res 53: 728–741.
40. Stout AK, Raphael HM, Kanterewicz BI, Klann E, Reynolds IJ (1998) Glutamate-induced neuron death requires mitochondrial calcium uptake. Nat Neurosci 1: 366–373.
41. Pivovarova NB, Nguyen HV, Winters CA, Brantner CA, Smith CL, et al. (2004) Excitotoxic calcium overload in a subpopulation of mitochondria triggers delayed death in hippocampal neurons. J Neurosci 24: 5611–5622.
42. In t' Veld BA, Ruitenberg A, Hofman A, Launer LJ, Van Duijn CM, et al. (2001) Nonsteroidal anti-inflammatory drugs and the risk of Alzheimer's disease. N Engl J Med 345: 1515–1521.
43. Townsend KP, Praticò D (2005) Novel therapeutic opportunities for Alzheimer's disease: focus on nonsteroidal anti-inflammatory drugs. FASEB J 19: 1592–1601.
44. Weggen S, Eriksen JL, Das P, Sagi SA, Wang R, et al. (2001) A subset of NSAIDs lower amyloidogenic Abeta42 independently of cyclooxygenase activity. Nature 414: 212–216.
45. Eriksen JL, Sagi SA, Smith TE, Weggen S, Das P, et al. (2003) NSAIDs and enantiomers of flurbiprofen target gamma-secretase and lower $A\beta_{42}$ in vivo. J Clin Invest 112: 440–449.
46. Mahmud T, Rafi SS, Scott DL, Wrigglesworth JM, Bjarnason I (1996) Nonsteroidal antiinflammatory drugs and uncoupling of mitochondrial oxidative phosphorylation. Arthritis Rheum 39: 1998–2003.
47. Kirichok Y, Krapivinsky G, Clapham DE (2004) The mitochondrial calcium uniporter is a highly selective ion channel. Nature 427: 360–364.
48. Tu H, Nelson O, Bezprozvanny A, Wang Z, Lee SF, et al. (2006) Presenilins form ER Ca^{2+} leak channels, a function disrupted by familial Alzheimer's disease-linked mutations. Cell 126: 981–993.
49. Nelson O, Tu H, Lei T, Bentahir M, De Strooper B, et al. (2007) Familial Alzheimer disease-linked mutations specifically disrupt Ca^{2+} leak function of presenilin 1. J Clin Invest 117: 1230–1239.
50. Stutzmann GE, Smith I, Caccamo A, Oddo S, Parker I, et al. (2007) Enhanced ryanodine-mediated calcium release in mutant PS1-expressing Alzheimer's mouse models. Ann N Y Acad Sci 1097: 265–277.
51. Zatti G, Burgo A, Giacomello M, Barbiero L, Ghidoni R, et al. (2006) Presenilin mutations linked to familial Alzheimer's disease reduce endoplasmic reticulum and Golgi apparatus calcium levels. Cell Calcium 39: 539–550.
52. Rizzuto R, Pinton P, Carrington W, Fay FS, Fogarty KE, et al. (1998) Close contacts with the endoplasmic reticulum as determinants of mitochondrial Ca^{2+} responses. Science 280: 1763–1766.
53. Geula C, Bu J, Nagykery N, Scinto LF, Chan J, et al. (2003) Loss of calbindin-D28k from aging human cholinergic basal forebrain: relation to neuronal loss. J Comp Neurol 455: 249–259.
54. Palop JJ, Jones B, Kekonius L, Chin J, Yu GQ, et al. (2003) Neuronal depletion of calcium-dependent proteins in the dentate gyrus is tightly linked to Alzheimer's disease-related cognitive deficits. Proc Natl Acad Sci USA 100: 9572–9577.
55. Núñez L, Sánchez A, Fonteriz RI, García-Sancho J (1996) Mechanisms for synchronous calcium oscillations in cultured rat cerebellar neurons. Eur J Neurosci 8: 192–201.
56. Murphy TH, Blatter LA, Wier WG, Baraban JM (1992) Spontaneous synchronous synaptic calcium transients in cultured cortical neurons. J Neurosci 12: 4834–4845.
57. Brewer GJ, Torricelli JR, Evege EK, Price PJ (1993) Optimized survival of hippocampal neurons in B27-supplemented Neurobasal, a new serum-free medium combination. J Neurosci Res 35: 567–576.
58. Pérez-Otaño I, Luján R, Tavalin SJ, Plomann M, Modregger J, et al. (2006) Endocytosis and synaptic removal of NR3A-containing NMDA receptors by PACSIN1/syndapin1. Nat Neurosci 9: 611–621.
59. Bottestein JE, Sato GH (1979) Growth of a rat neuroblastoma cell line in serum-free supplemented medium. Proc Natl Acad Sci USA 76: 514–517.
60. Xie L, Johnson RS, Freeman RS (2005) Inhibition of NGF deprivation-induced death by low oxygen involves suppression of BIMEL and activation of HIF-1. J Cell Biol 168: 911–920.